Chapter 15
HgCdTe Device Technology

Sergey Alekseevich Dvoretsky, Vladimir Vasilievich Vasiliev, George Yurievich Sidorov, and Dmitriy Vitalievich Gorshkov

15.1 Introduction

Over the past few decades, solid solution of ternary mercury cadmium telluride (MCT, HgCdTe) has demonstrated its excellent photoelectric performance for numerous infrared (IR) applications in "technical vision" systems. HgCdTe ranks first among a variety of solid-state photosensitive materials for the design and manufacture of IR detectors due to its unique physical properties, such as bandgap change over a wide spectral range, high absorption coefficient, high mobility, and carrier life. High-quality HgCdTe IR detectors successfully operated in three important atmospheric transparency windows: SWIR (1–3 μm), MWIR (3–5 μm), and LWIR (8–14 μm), as well as in VLWIR (over 14 μm) and THz spectral ranges.

Scientific research of technological processes was carried out to implement high-quality parameters of various HgCdTe IR detectors, determined by the background-limited performance (BLIP). The developed technologies represent a database of the developer companies, which is used for the development of specific focal plane arrays (FPA) for the infrared range and subsequent optimization of their performances. The scientific basis of technological processes of various manufacturers of IR HgCdTe detectors does not differ greatly. However, the application of this knowledge in the development of a specific version of technological processes for the manufacture of IR FPA requires many additional experiments to obtain the parameters of specific technological operations and their sequence to ensure the optimal technology. The choice of chemicals, required temperatures for technological processes, equipment, etc. determines the uniqueness of HgCdTe IR detector technology of each developer and generates its know-how. This, in turn, provides such technologies with the competition in the market. The rapid growth of the

S. A. Dvoretsky (✉) · V. V. Vasiliev · G. Y. Sidorov · D. V. Gorshkov
Rzhanov Institute of Semiconductor Physics, Novosibirsk, Russia
e-mail: dvor@isp.nsc.ru; vas@isp.nsc.ru; george@isp.nsc.ru; gorshkovdv@isp.nsc.ru

G. Korotcenkov (ed.), *Handbook of II-VI Semiconductor-Based Sensors and Radiation Detectors*, https://doi.org/10.1007/978-3-031-19531-0_15

market of HgCdTe IR detectors is associated with the expansion of their field of application, which requires single or small-format FPAs with a number of pixels up to tens of thousands, up to unique megapixel matrices up to 17,000,000 pixels, and, as a consequence, a large number of technologies.

Nevertheless, given the uniqueness and compliance with the know-how of the parameters of technological processes, the enormous information about the studies of HgCdTe IR FPAs in the articles does not give detailed ideas about the technology of their fabrication, let alone reproduction. There is only a general idea of how to develop an HgCdTe technology that satisfies such requirements as (1) the possibility of forming the required architecture of the photodetector, (2) creating conditions that ensure the manufacture of photosensitive pixels with the required size and spectral range of sensitivity, (3) the possibility of manufacturing photodetector matrices of the required format, (4) the possibility of passivating pixels and ensuring the stability of their parameters, and (5) creating ohmic low-resistance electrical contacts for outputting a signal from a pixel, etc.

The main modes of operation of IR photodetectors based on HgCdTe, which is a direct gap semiconductor, are photoconductive and photoelectric modes. The latter approach, using the formation of p-n junctions or heterojunctions, is currently the main direction in the development of infrared detector technologies based on HgCdTe. In this chapter the technologies for the manufacture of a photovoltaic matrix photosensitive element based on HgCdTe will be considered. We will discuss the HgCdTe material technology, p-n junction formation technologies, wet and dry etching technologies used for the matrix photosensitive element formation, passivation technologies by a deposition of dielectric layers, and the requirement for electric contacts used in photodetectors.

15.2 HgCdTe Material Technology

The HgCdTe material technology has gone through a consistent path of development from the bulk crystals to various epitaxial technologies. The evolution of the technology of photosensitive HgCdTe material, considered in [1, 2], is shown in Fig. 15.1. According to this figure, published in 2009, bulk crystal technology has not yet been developed. But it should be noted that the interest in bulk crystals has not been lost, and now single crystals of HgCdTe are produced in the required quantities.

15.2.1 HgCdTe Bulk Crystal Technology

The photosensitive HgCdTe material for IR detectors appeared in 1959. Lawson [3] and Schneider [4] synthesized the first HgCdTe bulk crystals. This research led to a real revolution in infrared photoelectronics. It was shown that in the CdTe/HgTe

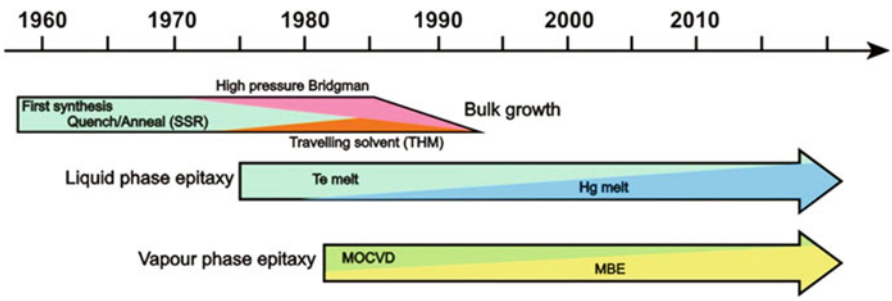

Fig. 15.1 Evolution of the technology of photosensitive HgCdTe material. (Data extracted from Refs. [1, 2])

system, both compounds have infinite solubility with respect to each other and form a continuous series of solid solutions with a change in the bandgap in a wide range of the IR spectrum. Since the 1960s, with such impressive results, HgCdTe bulk crystal technology has been expanded through the development of various growth methods. The common requirements for obtaining the high-quality HgCdTe bulk crystal are the following:

- High purity of initial materials Cd, Te, and Hg, which will provide a low residual impurity level and controlled intentional impurity doping to stabilize a low level of electron photoconductor-based detectors and required hole concentration for photodiodes.
- Equipment to ensure the growth processes taking into account a high pressure of mercury during the crystallization of HgCdTe bulk crystals.
- Crucible materials and equipment must ensure minimal interaction with the initial materials and their compounds at high temperatures.

Bulk crystal technologies associated with HgCdTe are summarized by Capper in [5–8] based on data in [6–11] and are based on three basic methods: solid-state recrystallization (SSR), traveling heater method (THM), and Bridgman methods.

15.2.1.1 Solid-State Recrystallization Method

In the solid-state recrystallization (SSR) method developed in the United States, pure elements Hg, Cd, and Te are loaded into an etched silica ampoule and mixed in the melt at elevated temperature [9]. Then the homogeneous melt of Hg, Cd, and Te is rapidly quenched into air or oil up to room temperature. As a result of this process, a dendritic structure is formed. To obtain single-crystal grains, subsequent recrystallization of the synthesized material is required, carried out at temperatures below the solidus line for a long time. Various methods have been proposed for reducing the density of defects or eliminating the causes of their appearance in the synthesized material in SSR processes. For preparing n-type HgCdTe, the grown p-type material is converted to n-type material by thermal annealing in an Hg atmosphere. The

precipitation of second phase formed in the ingot of HgCdTe can be minimized by increasing the partial pressure of Hg and slowing down the cooling process after reheating the slices, while encapsulating in another ampoule of silica. In this case, the dislocation density can be decreased to two orders of magnitude.

15.2.1.2 Traveling Heater Method

Traveling heater method (THM) developed in France was presented by Triboulet in [10]. In this method, the molten zone slowly moves through the solid homogeneous source material (polycrystalline HgCdTe) as the ampoule moves through the heater. During this process, dissolution of the material in the hot state and crystallization of HgCdTe of the same composition at cold interfaces are observed in the temperature gradient under steady-state conditions. The melt zone partially purifies the material during the TMH process. THM makes it possible to grow longer and larger bulk HgCdTe crystals up to 40 mm in diameter.

15.2.1.3 Bridgman Method

In the Bridgman process developed in the United Kingdom [8], pure elements Cd, Hg, and Te are loaded into a purified silica ampoule and then are homogenized, while heating to the melting state. Upon cooling, starting from the end of the ampoule of a certain configuration, a large-grained ingot was grown. To reduce radial temperature fluctuations, a slow rotation around the vertical axis was used. To prevent accidental explosions, which can be caused by a pressure of 70 atm arising in the ampoule upon rapid heating, the ampoule for the growth of HgCdTe crystals was placed in an additional semi-hermetic cell. The accelerated crucible rotation technique (ACRT) is used to maintain the composition uniformity. The largest crystal up to 70 mm in diameter was grown by the Bridgman method (see Fig. 15.2). It is seen that the crystal structures degenerate with increasing diameter.

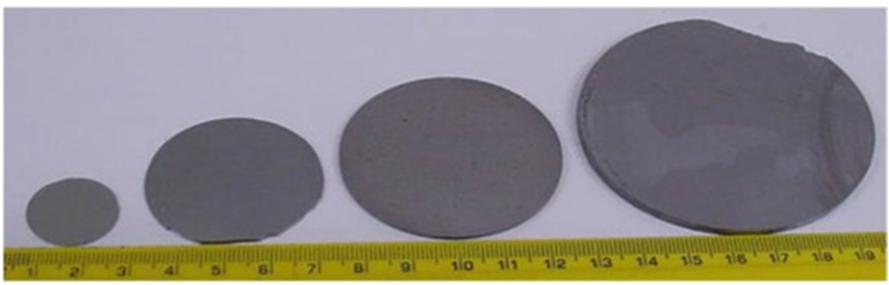

Fig. 15.2 HgCdTe wafers of different diameter grown by Bridgman process. (Reproduced with permission from Capper [8]. Copyright 2017 Springer)

In the former USSR (now in Ukraine), a HgCdTe bulk crystal, 50 mm in diameter, was grown by the method of melt crystallization of HgCdTe solid solution [12]. The composition of homogeneous HgCdTe solid solution corresponded to the solidus temperature. The HgCdTe bulk crystal was doped with In with concentration of (2–4) × 10^{14} cm^{-3} to a stabilized donor level. The dislocation density was ~3 × 10^5 cm^{-2} for HgCdTe doped with In and ~10^4 cm^{-2} for isovalent doping with Se. After the growth of a bulk HgCdTe crystal, a concentration of Hg vacancies of (1–10) × 10^{17} cm^{-3} and Te precipitations is observed. After thermal annealing at ~400 °C and further annealing at 250–280 °C in a saturated atmosphere of Hg, a homogeneous HgCdTe bulk crystal can have p-type or n-type conductivity with a carrier concentration of (5–20) × 10^{15} cm^3 and (2–4) × 10^{14} cm^{-3}, respectively.

15.2.2 HgCdTe Epilayer Technologies

Bulk crystal technology of HgCdTe with n-type and p-type conductivity makes it possible to create single-crystal substrates for fabrication of small-sized photoconductors and photovoltaic infrared detectors aimed for application in thermal imaging systems. To increase the visibility range and more accurate spatial resolution, which can be achieved through the use of large-format IR photodetector arrays, epitaxial technologies for growing HgCdTe layers on various large-diameter substrates have been developed. Epitaxial layers have an optimal thickness for absorption of radiation, the required electrophysical parameters, and a minimum number of defects. Heteroepitaxial structures (HES) made of HgCdTe grown on various substrates are a "semi-finished product" that significantly improves and simplifies the technology for fabricating devices based on HgCdTe. The first technology for growing epitaxial layers of HgCdTe was liquid-phase epitaxy (LPE), which was the simplest method suitable for this purpose. However, to carry out LPE processes, it was necessary to use only isovalent single-crystal substrates, such as CdTe, which was used at the initial stage and was subsequently replaced by CdZnTe.

15.2.2.1 Liquid-Phase Epitaxy

At present time, LPE is the most developed epitaxial technology for growing high-quality homogeneous HgCdTe epitaxial layers. Due to the relative simplicity and high manufacturability of LPE, the HgCdTe technology has been introduced in the industrial production. The main advantages of LPE technology are the following:

- Relatively low cost and high performance of the equipment
- Relatively low growth temperatures of 450–550 °C
- Uniform distribution of the composition over the area
- High crystal perfection
- Required electrophysical parameters

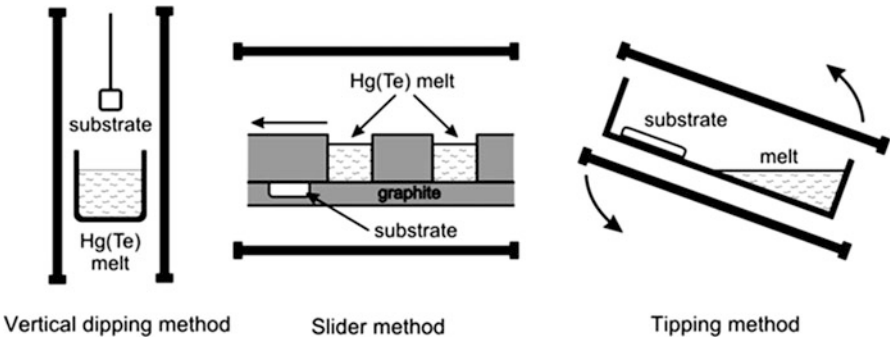

Fig. 15.3 The scheme of decantation in dipping (*left*), slider (*in the center*), and tipping (*on right*) types of LPE technologies

The analysis of the Cd-Hg-Te-phase diagram determined the main directions of the LPE technology development based on the use of Te- or Hg-rich melts. In connection with the use of various solvents, the development of LPE technology was carried out by various methods, such as:

- Horizontal open-tube slider method
- Vertical dipping method
- Tipping method in a closed sealed quartz ampoule

The important key problems of the LPE method are associated with removing a residual melt from the epitaxial layer surface (decantation) and maintaining a given liquid-phase composition [13]. The scheme of decantation at different LPE techniques is shown in Fig. 15.3. In a horizontal slider-type LPE, the decantation is carried out by shifting the melt from the epitaxial layer surface by moving the parts of the graphite boat relative to each other. In a vertical dipping-type LPE, the melt flows free down from the surface under the gravity force. In a tipping-type LPE, the revolute architecture is used to free the melt removal or in combination with a slide. In [14, 15] it was shown that there are difficulties at the decantation of Te-rich melt because of its viscosity and the low surface tension value. Thus, the existence of residual melt drops is possible on the surface. It was proposed to carry out centrifugation to completely remove the Te-rich melt from the surface of the epitaxial layer surface at the growth in a sealed ampoule. An important problem of LPE is associated with the uniformity of the HgCdTe composition over the thickness of the epitaxial layer. Hg evaporates from the melt during epitaxial processes, resulting in uncontrolled composition of the growing HgCdTe layer. In a slider-type LPE with a Te-rich melt, the loss of Hg is replenished by adding Hg vapor to the hydrogen flow [14, 16] or HgTe to the melt [15, 17, 18].

Various designs of quasi-hermetic boats based on high-purity and dense graphite have been developed [19, 20]. In the dipping-type LPE technology based on the Hg-rich and Te-rich melt [16, 21], the growth of large-area homogeneous HgCdTe layers is carried out from a very large melt volume called as “infinite melt” method

[22]. It was shown that the HgCdTe layers of high composition reproducibility x = 0.223 ± 0.001 (further x means CdTe mol. fr. in $Hg_{1-x}Cd_xTe$) over 54 cm^2 area in 200 LPE runs were grown from a 4–4.5 kg Te-rich melt [23]. For Hg-rich melts, the growth processes were carried out using a large mass of melt, up to 10 kg, with a decrease in temperature in the range of 200–245 °C [24–26]. The problem of changing the composition in the epitaxial layer during the growth in the closed tipping-type method is absent due to the constancy of the melt composition The Te-rich melt decantation using the revolute architecture and centrifugation was applied in [27–29]. When growing in a sealed ampoule, it was proposed to replace the CdTe substrate and to use two temperature zones of the furnace to enrich the Te-rich melt with Hg [30].

The characteristics of the HgCdTe HES material grown by the LPE method on (111) A, (111) B, (100) and misoriented from single-crystal CdZnTe substrates were studied by various physical methods. The presence of threaded and screw dislocations, as well as micron and submicron Te precipitates in epitaxial layers of HgCdTe grown from a Te-rich melt of sliding type [17, 31], dipping type [16, 32] and Hg-rich melt dipping type [26], and closed system tipping type [27], regardless of the growth method, was found. The dislocation density decreased from the interface to the surface throughout the entire thickness and reached a constant value (5–50) × 10^4 cm^{-2}. Thus, it was found that the dislocation densities on the surface are determined by the dislocation density in the substrate and are practically independent of the substrate/layer-matching conditions in the LPE method [33, 34]. Te precipitates in LPE epitaxial layers are localized, as a rule, near the interface and at the surface. The dependence of precipitate value on the growth conditions and the substrate misorientation from the (111) plane was found [32]. The specific feature of the surface morphology of the HgCdTe LPE epitaxial layer grown from a Te-rich melt is the presence of terraces, which is determined by the misorientation from optimal orientation (111) [16, 17, 32]. It is shown that the number of terraces decreases and a smoother surface is observed for misoriented substrates on 1.2–2 degrees from (111) A and (111) B. In addition, the smoothest and crystal-perfect layers are obtained at a minimum interval and cooling rate [16, 18]. The undoped LPE epitaxial layers, grown from Te-rich melts at 450–550 °C, have the p-type conductivity with the hole concentration and mobility (0.5–2.0) × 10^{17} cm^{-3} and (150–300) cm^2V^{-1} s^{-1} at 77 K, respectively. It is necessary to provide a low-temperature thermal annealing in the Hg vapor in order to reduce the concentration of holes or convert the material from p-type to n-type conductivity. The highlighting of experimental results was presented in [35–39]. The following two types of annealing are used: (a) under Hg vapor pressure control and (b) under Hg saturated vapor pressure. It was found that the concentration of holes decreased to optimal values (0.5–2.0) × 10^{15} cm^{-3}, and the mobility was at least 300 cm^2V^{-1} s^{-1} at 77 K when the thermal annealing temperature decreased. At a certain temperature of thermal annealing, the p-type conductivity was converted to n-type. This temperature depended on the growing conditions for HgCdTe LPE epitaxial layers and varied in the range of 230–330 °C. In this case, the electron concentration differs in different samples by an order of magnitude. In the purest HgCdTe LPE epitaxial

layers, after the thermal annealing at 260 °C during 100 hours, the electron concentration of 5×10^{13} cm^{-3} at 77 K was reported in [27]. The intentional HgCdTe doping during LPE growth makes it possible to significantly increase the reproducibility of the required electrophysical properties. A detailed analysis of the doping technology is presented in [40]. Very efficient doping was carried out with In, which provided ~100% degree of ionization and controlled electron concentration in the range $(1.0–50) \times 10^{14}$ cm^{-3} [22, 24, 27].

15.2.2.2 Metal-Organic Vapor-Phase Epitaxy

The results on growing HgCdTe layers using a metal-organic compound (MOVPE, MOCVD) by direct HgCdTe growth were first published in 1981 [41]. However, the method of direct growth of the HgCdTe layers did not allow obtaining the required quality of these layers, which is determined by the growth conditions during deposition process. Significant progress has been achieved only with the application of the MOCVD method, which is called the interdiffusion multilayer process (IMP) [42]. When using IMP method for HgCdTe layer growth, thin double layers of CdTe/HgTe, each 0.1–0.2 μm thick, are deposited with repetition and interdiffusion at the growth temperature. The composition of HgCdTe layer is changed by changing the ratio of CdTe and HgTe layers' thicknesses. Schematic cross section of the Aixtron AIX-200 reactor for the MOCVD HgCdTe growth is shown in Fig. 15.4 [43].

The HgCdTe layers were grown on 2 inch epiready, oriented 2° off (100) GaAs substrates to (110) in horizontal MOCVD reactor with H_2 carrier gas by the IMP process, using the following precursors: diisopropyl telluride (DiPTe), dimethyl

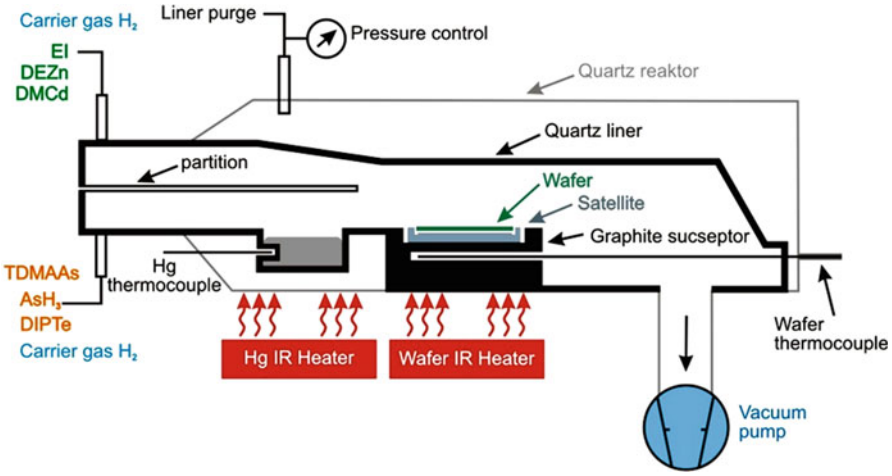

Fig. 15.4 Schematic cross section of the Aixtron AIX-200 reactor. (Reproduced with permission from Piotrowski et al. [43]. Copyright 2007 Springer)

cadmium (DMCd), and elemental mercury. A tris-dimethylamino arsenic (TDMAAs, $As[N(CH_3)_2]_3$) was used to control acceptor doping in the 10^{14}–5×10^{17} cm^{-3} range. An ethyl iodide (EI) was used for control donor doping in the 10^{14} cm^{-3}–1×10^{18} cm^{-3} range. The substrate temperature was kept at 350 °C and mercury zone at 210 °C. Tellurium flush during nucleation process provided (111) CdTe growth. Surface morphology of (111) HgCdTe was improved by thermal annealing of GaAs substrate at 600 °C in hydrogen flow before Te nucleation [44]. The II/VI mole ratio was kept in the range from 1.5 to 5 during CdTe cycles of the IMP process. Typically, 3–4-μm-thick CdTe layer was used as a buffer layer, reducing stress caused by crystal lattice misfit between GaAs substrate and HgCdTe epitaxial layer structure. The given MOCVD setup (scheme in Fig. 15.4) and the technological process describe the MOCVD technology.

However, there are differences in MOCVD technology developed by other researchers and manufacturers. Various MOCVD settings, precursor materials, specific cultivation processes, substrates, etc. determine these differences. GaAs substrates have proven to be the preferred substrates for growing high-quality MOCVD HgCdTe layers over large areas. The Si substrate is more attractive than the GaAs substrate. However, it is very difficult to implement the MOCVD HgCdTe technology on Si substrates due to the problem of in situ removal of thermal oxides. The optimal thickness of the CdTe buffer layer on the GaAs substrate for achieving high crystal quality and reducing the gallium doping level was determined in [44, 45]. This makes it possible to reduce the defect density and improve the quality of the HgCdTe epitaxial layers [46]. The orientation of the substrate should provide HgCdTe layers with a mirror-smooth surface, a minimum number of macrodefects, and the required doping level.

In Great Britain and Poland, the preferred orientation for MOVPE growth of HgCdTe is still misoriented (100) GaAs [44]. In the United States, (211)B CdZnTe substrates are the preferred orientation for MOCVD. In Russia, GaAs substrates with orientation (100) and (310) are used [47]. Surface roughness depends on the orientation of the substrate, surface preparation, and the nucleation process at the initial stage of growth. Although the surface roughness for (211)B HgCdTe is about half that for (111)B HgCdTe, the latter orientation gives the progress in improving the parameters of the IR detector. Growth temperatures for the IMP method range from 230 to 410 °C and are determined by the initial choice of metal-organic compounds (MOCs) [48–50].

The use of photostimulated and plasma-stimulated decomposition of MOCs in the gas phase allows the growth temperature to be reduced to 150 °C and 135 °C, respectively [51]. The IMP method makes it possible to obtain multilayer heterostructures with different designs of composition and doping distribution over the thickness, mirror-like surface morphology, and uniformity of HgCdTe composition over the surface area. This makes it possible to provide the processes of thermal annealing and deposition of a passivation coating in one growth cycle. In MOCVD, as in MBE, layer thickness and precursor concentration can be monitored using ellipsometry and in situ laser reflectometry [43, 52]. All this makes it possible to manufacture large-area IR focal plane photodetector arrays (FPAs) based on

MOCVD HgCdTe layers with high operating parameters [5, 53]. The main disadvantage of the MOCVD HgCdTe technology is the toxicity of original precursors used during this process.

Studies of the behavior of impurities in epitaxial HgCdTe MOCVD epitaxial layers are presented in [54–57]. It was found that Ga, In, Al, and I exhibit donor properties, while P, As, and Sb exhibit acceptor properties. The most widely used impurities for obtaining n-type and p-type conductivities are I [43] and As [57, 58]. In the IMP, the doping with As is carried out during the growth of the CdTe layer and, as a rule, with an excess of Cd in the gas phase [58, 59]. The arsenic precursor AsH_3 provides almost 100% electric activities of As. However, due to its toxicity, other arsenic precursors have been considered. In the case of the precursors, such as trimethylarsine ($(CH_3)_3As$) and diethylarsine ($(C_2H_5)_2AsH$), doping with As led to its concentrations below 10^{16} cm^{-3} and low electrical activation [60] or to the formation Shockley-Read-Hall (SRH) recombination centers [3]. The most promising precursor for doping HgCdTe with arsenic is TDMAA, which, upon decomposition with the formation of atomic As, makes it possible to obtain 100% electrical activation of arsenic [43, 61].

The lifetime of minority carriers in HgCdTe doped with As from TDMAAs is an order of magnitude higher than lifetime in HgCdTe doped with other metal-organic precursors and is limited only by fundamental recombination processes [62]. It is important that the composition of the grown HgCdTe layers depends on the precursor used for doping. For example, a decrease or an increase (10% ($x \sim 0.2$)) was observed in the composition of the HgCdTe layers upon doping with As from AsH_3 or TDMAA, respectively. A significant increase in the composition of HgCdTe was also observed upon HgCdTe doping with $InMe_3$ and $AsMe_3$, and a decrease in the case of $SbMe_3$ [63].

15.2.2.3 Molecular Beam Epitaxy

Significant possibilities to realize the unique properties of HgCdTe for different applications, both in the traditional direction in the development of IR technology devices and in the direction of development of devices based on quantum phenomena, are associated with the technology of growing HgCdTe structures by molecular beam epitaxy (MBE). MBE is a very modern flexible technology and is widely developed due to the following advantages:

- Minimal low growth temperature (160–200 °C), which provides sharp interfaces between layers, a low background impurity doping level below 10^{11} cm^{-3}, and a low impurity diffusion from the substrate
- Absence of an aggressive medium, which allows using alternating Si, GaAs, and Ge substrates large in diameter
- Monitoring of growth processes by different electron and optical tools in situ
- Growth processes of multilayer HgCdTe HES with a required composition design and doping throughout the entire thickness, including CdTe/HgTe superlattices, HgCdTe/HgTe/HgCdTe quantum wells, and other nanostructures.

Ultrahigh vacuum (UHV) MBE setups have been developed for growing Hg-containing compounds and, first of all, HgCdTe HES using MBE technology. The latest generation of UHV MBE setups allows growing HgCdTe HES on 1 × 150 (200) mm (6″(8″)), 4 × 100 mm, or 5 × 76.2 mm substrates, such as MBE 49, RIBER 412, Veeco 20, and VG Semicon V-100, which advance the HgCdTe growth. In the Rzhanov Institute of Semiconductor Physics, Siberian Branch of Russian Academy of Sciences (ISP SB RAS), a multiple-chamber UHV MBE setup "Ob'-M" was developed for the growth of HgCdTe HES without rotation of 100 mm in diameter substrates [64]. All UHV MBE setups are equipped with oil-free pumps to obtain a residual gas pressure of less than 10^{-9} Pa. Technological chambers are equipped with molecular beam sources, usually Knudsen type, for basic and doping materials, a manipulator with heaters, and analytical equipment for monitoring the growth processes, such as reflection high-energy electron diffraction (RHEED), spectral ellipsometry and single-wavelength ellipsometry in situ, and vacuum and temperature gauges. The ellipsometry monitoring does not affect the growth processes over RHEED, especially in case of HgCdTe, and provides a high-accuracy monitoring in situ of the substrate temperature, composition, growth rate, thickness, and surface roughness [65–67]. To obtain a high uniformity of HgCdTe layer's composition, thickness, and doping level over the surface area during growth on large-diameter substrates, it is necessary to rotate the substrate, which limits the application of monitoring in situ. Large volume ring-type Cd and Zn, Knudsen-type Te molecular beam sources, and a ring-type Hg flux former coaxially designed together provide high composition uniformity over the surface without substrate rotation (Fig. 15.5) [68].

The Te molecular beam source has a low-temperature evaporation zone and a high-temperature zone of flux formation at the outlet. Cd and Zn molecular beam sources and Hg flux former have a narrow aperture outlet [69]. The proposed design of the technological unit allows obtaining the HgCdTe composition uniformity over the substrate area without substrate rotation, compared with the best-published data. CdZnTe, GaAs, Ge, and Si are used as the basic substrates for the growth of HgCdTe HES by MBE. CdZnTe substrates provide the growth of high-quality HgCdTe HES for IR FPAs operated in important spectral ranges, such as 1–3 μm (SWIR), 3–5 μm (MWIR), 8–14 μm (LWIR), and over 14 μm (VLWIR). But at present, preference is given to larger-area GaAs, Ge, and Si substrates from the point of view of a significant reduction in material cost and subsequent costs for MFP. Despite the high mismatch of crystal lattices between HgCdTe and GaAs, Ge, and Si, numerical studies make it possible to develop MBE technologies for high-quality growth of large-area HgCdTe HES on such substrates. The low growth temperatures of HgCdTe and the strong dependence of the mercury sticking coefficient [70] require the choice of orientation to obtain high-quality layers [71]. Studies of the growth of HgCdTe on (100), (111)B, (211)A, (211)B, and (013) substrate orientations showed that better surface morphology, the absence of twins, and higher sticking coefficients are achieved through the use of (211)B and (013) orientations [72, 73]. To maintain the initial substrate orientation and eliminate a large lattice mismatch between Si, GaAs, Ge, and HgCdTe, it is necessary to grow, sequentially, a buffer layer of ZnTe and CdTe for creating alternative CdTe/ZnTe/Si (GaAs, Ge) substrates [74–76].

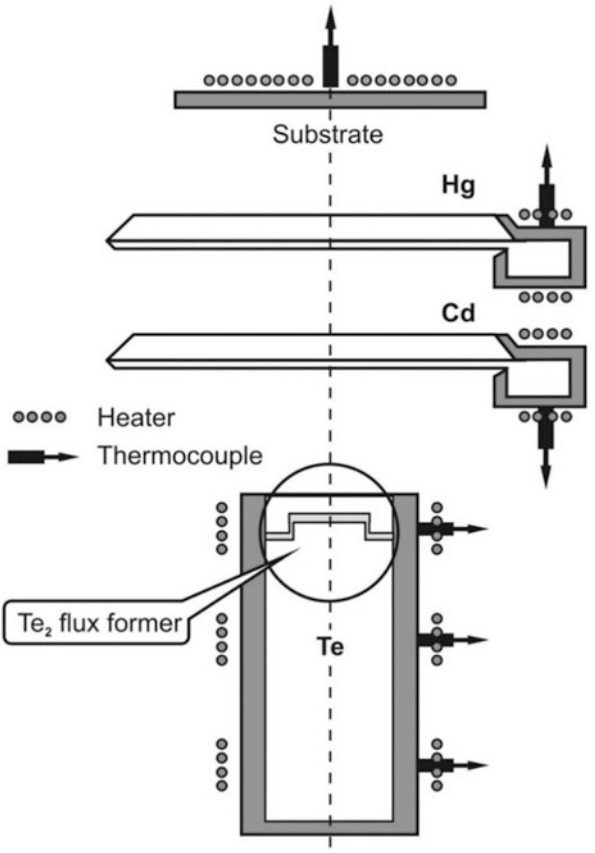

Fig. 15.5 The scheme of Cd and Zn ring-type and Te Knudsen-type molecular beam sources and Hg flux former location in HgCdTe deposition chamber

Before growing, the surface substrates were prepared by liquid chemical etching (no need for epiready) and thermal cleaning in a vacuum. All substrates were cleaned in an organic solvent. This is followed by chemical etching of CdZnTe in 0.5–1 vol. % Br/methanol [5], Ge in the H_3PO_4:H_2O_2:H_2O solution [76], GaAs in the H_2SO_4/H_2O_2/H_2O [77] with the following treatment in the HCl:isopropanol solution, and Si – in RCA, based on HF. Thermal annealing of CdZnTe substrates in ultrahigh vacuum was carried out at 220 °C to remove the passivating layer of Te, Ge annealing at ~650 °C to remove oxides in As flux, annealing of GaAs substrates at ~580 °C to remove oxides (in case of epiready) [78] or the As passivation layer, and Si annealing at 550–600 °C to remove the hydrogen passivation layer. The last technological procedure for creating an atomically clean and smooth substrate surface before growing HgCdTe is necessary for growing at 200–320 °C a thin CdTe layer on a CdZnTe substrate, as well as a thin ZnTe and a thick CdTe buffer layer on Ge, GaAs, and Si substrates [5, 77, 78].

The (211)B HgCdTe/CdZnTe HES technology on a (8x8) cm^2 CdZnTe substrate was developed in Teledyne [79] and Raytheon [80]. The growth of the HgCdTe layer is carried out at T ~ 180–190 °C from the sources of Te, CdTe, Hg, In, and As. The obtained HgCdTe HES had the following parameters: $x = 0.2072 \pm 0.0021$ (cutoff wavelength $\lambda_c = 11.0 \pm 0.1$ μm at 78 K), thickness 13.26 ± 0.06 μm; the electron concentration ranged from 10^{14} to 10^{16} cm^{-3}, and the density of macrodefects was less than 10 cm^{-2} for sizes exceeding 10 microns, less than 10^3 cm^{-2} for sizes 4–10 μm, and less than 10^4 cm^{-2} for sizes less than 4 μm. The dislocation density was less than 5×10^5 cm^{-2}. In Sofradir, the technology (211)B HgCdTe/Ge HES was developed on Ge substrates with a diameter of 100 and 125 mm with spectral ellipsometry control [84, 85]. The temperature distribution over the substrate was no worse than 3 °C and was kept in the process no worse than 0.25 °C. The following parameters of HgCdTe HES were obtained: mirror-smooth surface, density of macrodefects from 200 to 300 cm^{-2}, and density of dislocations from 5×10^6 to 2×10^7 cm^{-2}. 1280 × 1024 IR FPAs with a pixel size of 15 μm were manufactured with the following parameters: wavelength cutoff, 5.20 ± 0.04 μm; sensitivities, 7.7×10^9 V/W and 2.75 A/W; quantum efficiency, 70%; NETD, 19 mK; and operability, more than 99.8%. These results lead to the conclusion that HgCdTe/Ge HES technology provides a high quality of megapixel MWIR FPAs.

The (211)B HgCdTe/GaAs HES technology on 100 mm in diameter GaAs substrates was developed in AIM Infrarot [81]. The resulting MCT layers had the following parameters: the homogeneity of the composition of HgCdTe for the MWIR and LWIR spectral ranges was ±1% in area, the dislocation density was (2–3) × 10^7 cm^{-2}, and the density of macrodefects was 50 cm^{-2} with their size <10 μm and 4 cm^{-2} at a size >10 μm. The improvement of the technology was associated with the introduction of wide-gap passivation layers, which led to an improvement in the performance of IR 640x512 FPAs [81]. The Rzhanov Institute of Semiconductor Physics SB RAS has developed the (013)HgCdTe/GaAs HES technology on GaAs 3 inch substrates without rotation using the growth process control by single-wave ellipsometry [75, 82, 83]. The popular "semifinal" HgCdTe HES has wide-gap gradient layers ($x = 0.18$–0.32) at the absorber interface and the surface to simplify the technology of manufacturing IR detectors and improve their parameters (see Fig. 15.6). The concentration and mobility of electrons varied in the ranges 10^{14}–10^{15} cm^{-3} and (0.5–1.5) × 10^5 cm^2V^{-1} s^{-1}, respectively. The lifetime of minor charge carriers varied from 1 to 10 μs. The dislocation density was about 5×10^6 cm^{-2}. The p-type HgCdTe HES with hole concentrations (5–20) × 10^{16} cm^{-3} was obtained during the thermal annealing at 200–220 °C for 24 hours. The (211)HgCdTe/GaAs HES technology on Si 6 inch substrates was developed at Raytheon [86]. Growth temperature and molecular fluxes of Hg, Cd, and Te have been optimized to grow high-quality HgCdTe HES. The p+-n detectors, based on the double-layer heterojunction structures (DLHJ), were grown for single-spectral IR FPAs.

For MWIR HgCdTe HES, the composition uniformity was ~0.1% (the cutoff wavelength – ±0.2 μm); dislocation density, 5×10^6 cm^{-2}; and macrodefects

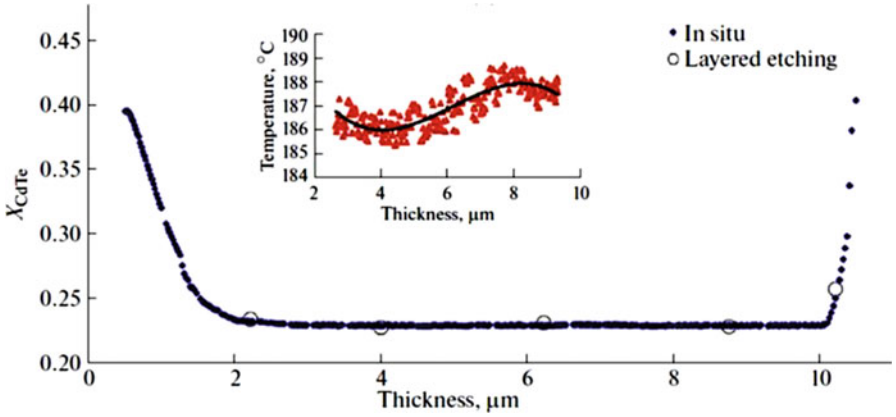

Fig. 15.6 The HgCdTe composition distribution throughout the thickness in HgCdTe layer with graded wide-gap layers on absorber interface and surface. Inset showed the temperature during the HgCdTe growth. The points are HgCdTe composition measured by transmission spectra with layer-by-layer etching. (Data extracted from Ref. [83])

density, less than 100 cm^{-2}. For 640 × 480 IR FPAs, the following high-sensitivity values were obtained: NETD 19 mK, operability 99.7% for MWIR, and NETD 22 mK, operability 99.3% for LWIR. Thus, it was shown that HgCdTe/Si layers provide IR FPAs a quality comparable to that based on HgCdTe/CdZnTe layers. Recently [87] reported impressive results of growing HgCdTe HESs on Si substrates 200 μm in diameter. Twin-free high-quality HgCdTe layers were obtained with the following HgCdTe HES parameters: composition, x = 0.2903 ± 2.2% (the cutoff wavelength – 5.26 ± 5%); thickness, (9–10) ± 0.33 μm; and macrodefects density, 22–170 cm^{-2}. The As concentration varied in range (1.5–3.5) × 10^{18} over a length of 100 mm from the center to the edge. A photograph of HgCdTe/Si structures grown on 6 and 8 inch Si substrates is shown in Fig. 15.7a.

The (013) HgCdTe/Si HES technology on Si substrates up to 4 inches in diameter was developed in Rzhanov Institute of Semiconductor Physics SB RAS for MWIR IR FPA [88, 89]. A photo of HgCdTe/Si structures grown on 4 inch Si substrates is shown in Fig. 15.7b. The HgCdTe HES had the following parameters: mirror-smooth surface; the density of macrodefects, less than 500 cm^{-2}; and thickness ~5 μm, x = (0.3–0.35) ± 0.002 (cutoff wavelength ~0.1 μm) at 77 K. As-grown undoped HgCdTe layers had n-type conductivity with electron concentration, mobility, and lifetime (5–10) × 10^{14} cm^{-3}, (15000–25,000) $cm^2V^{-1}c^{-1}$, and 5–15 μs, respectively. After thermal annealing HgCdTe layers had p-type conductivity with hole concentration, mobility, and lifetime (1–15) × 10^{15} cm^{-3}, (200–400) $cm^2V^{-1}c^{-1}$, and 3–50 ns, respectively. In P+-n DLHJ n-HgCdTe In-doped absorber had the following parameters: thickness ~5 μm, x = 0.29–0.31, and n = (1–10) × 10^{15} cm^{-3}. The p+-HgCdTe layers doped with As ions and two-step thermal annealing, first at 360 °C and then at 225 °C, had the following parameters: x = 0.35–0.6 and p = (1–10) × 10^{17} cm^{-3}. DLHJ structures are used for the manufacturing of large-

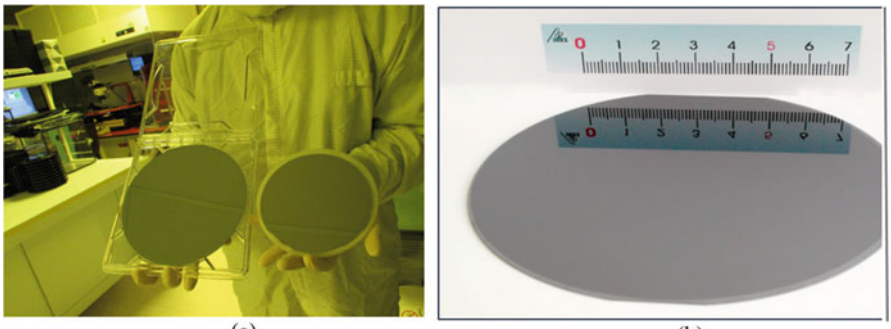

Fig. 15.7 The photograph of HgCdTe/Si structures: (**a**) 8″ in diameter and 6″ in diameter; (**b**) 4″ in diameter. ((**a**) Reproduced with permission from Reddy et al. [87]. Copyright 2019 Springer; and (**b**) from Yakushev et al. [88]. Copyright 2011 Springer)

format IR FPAs operating at elevated temperatures. It was shown that HgCdTe layers with a dislocation density of less than 5×10^5 cm^{-2} do not affect the photoelectric parameters of IR FPAs. HgCdTe/CdZnTe HES technology has low dislocation density and allows obtaining high-quality IR FPAs in wide spectral range. HgCdTe/Si(Ge, GaAs) HES technology has high dislocation density exceeding 5×10^6 cm^{-2}. Nevertheless, SWIR, MWIR, and LWIR IR FPAs based on HgCdTe/Si(GaAs, Ge) HES have sensitivity which is comparable to those based on HgCdTe/CdZnTe. For VLWIR IR FPAs, the sensitivity is an order of magnitude lower [90]. It was shown earlier that the dislocation density in the (211)HgCdTe/Si HES was decreased to 10^6 cm^{-2} by a fast thermal cycling during 1 min in the range 290–350 °C without a composition change [91]. Macrodefects on the surface in the form of hillocks or pits (voids, V-defects) determine the quality of HgCdTe HES and the performance of IR photodiodes [92]. V-defects inside p-n junctions are called "killers." It was found that the presence of V-defects near the p-n junction is the reason for the increase in the dark current. The reasons for the formation of V-defects are the crystallization of elemental tellurium during growth in places of deficiency of mercury and high temperatures [93–95].

It was shown that well-controlled n-HgCdTe in MBE technology is easily achieved by the intentional In doping in a wide range of 10^{14}–10^{19} cm^{-3} [96]. The introduction of Hg vacancies provides the obtaining of p-HgCdTe with the hole concentration in the range $(5–20) \times 10^{15}$ cm^{-3}. However, they are unstable to diffusion processes, reduce the hole mobility, and act as SRH recombination centers [97]. Group I elements show up to 100% activation upon doping during growth and exhibit excellent transport properties. However, such impurities quickly diffuse, both during growth and during thermal annealing, which does not allow the use of these impurities for obtaining a stable p-type and their application in the device technology. The low diffusion coefficient of As atoms allows the growth of stable, well-controlled p-type layers and p-n junctions. After growing, As-doped HgCdTe layers show their n-type conductivity [98]. For the conversion to p-type

conductivity, it is necessary to activate As for the insertion into Te vacancies. Several activation methods have been proposed. The standard activation method consists of a two-stage thermal annealing, first for 10 min at 425 °C and then for 24 hours at 250 °C, which leads to almost complete activation of As to a hole concentration of $\geq 10^{18}$ cm^{-3}.

15.3 Etching Technology

The HgCdTe etching material technologies are used in the mesa technology of manufacturing IR detector. It is necessary to divide pixels for cross-talking elimination that leads to the deterioration in the frequency-contrast characteristic. The etching technology can be carried out by using liquid-phase (wet) or gas-phase (dry) etchings.

In wet etching the solution of Br in HBr [99] or Br in methanol (Br/Me) [100] is used as a liquid etchant. The etching rate is determined with high precision by accurately controlling the concentration of the liquid etchant and the temperature. It was shown that the temperature affects the etching rate during technological process using a Br solution in HBr [101]. The linear dependence of the groove depth on the etching temperature is shown in Fig. 15.8. It was shown that the etching temperature in the range from −18 °C to +15 °C does not change the surface morphology.

It was shown that an etching rate of ~10 nm/min makes it possible to provide a groove depth of 50 ± 5 nm in HgCdTe with good accuracy. The disadvantages of wet etching include the following:

- Formation of an excess Cd layer on the surface of the HgCdTe grooves after both Br/HBr and Br/Me with cadmium oxide as the last etchant

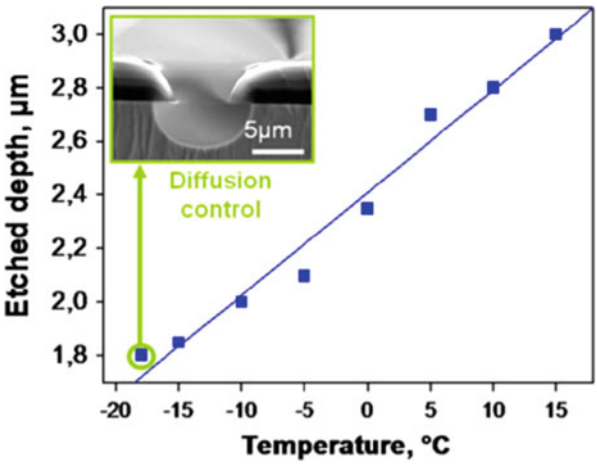

Fig. 15.8 The etched depth of HgCdTe vs. temperature. The inset shows a scanning electron micrograph of the groove etched at −18 °C. (Reproduced with permission from Causier et al. [101]. Copyright 2011 Springer)

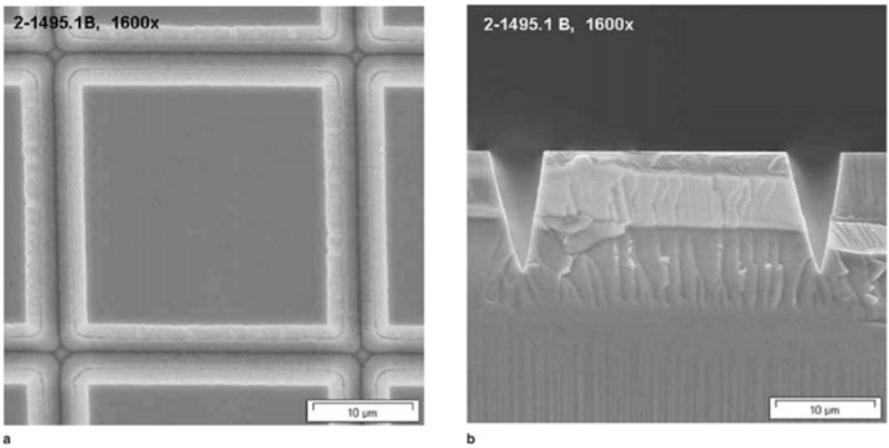

Fig. 15.9 The SEM photo of 30 × 30 µm diode area after dry etching using inductively coupled plasma (ICP): (**a**) top view; (**b**) cleaved lateral face. The mesa depth is approximately 15 µm. The photoresist is used at etching process and then removed. (Reproduced with permission from Cmith et al. 2003. Copyright 2003 Springer)

- Anisotropic nature of groove etching (see inset in Fig. 15.8)
- Reduction of pixel sizes at large groove depth

Dry etching technological processes, using ionic and plasma-chemical modes have been intensively developed. In the ionic mode, Ar gas is used to create ions for the etching process [102, 103]. In the plasma-chemical mode, the following gas mixtures are used: $Ar + H_2$ [99, 104], $CH_4 + H_2$ [99], $CH_4 + Ar$ [99], $CH_4 + H_2 + Ar$ [99, 104], $H_2 + Ar + N_2$ [99], and $CH_4 + H_2 + N_2 + Ar$ [104]. In the case of the $CH_4 + H_2 + Ar$ gas mixture, $Te(CH_3)_2$, TeH_2, $Cd(CH_3)$, and Hg were formed as etching products [105, 106]. However, in the case of the $H_2 + Ar$ gas mixture, etching products TeH_2 and Hg were formed [105]. This means that for etching Cd, a CH_3 radical is required. The SIMS studies show that the addition of N_2 to the $CH_4 + H_2$ gas mixture leads to the formation of NH_3 and HCN [106]. The addition of N_2 to the $CH_4 + H_2 + Ar$ gas mixture leads to a decreasing H concentration and an increasing in the CH_3 radical density [99, 107, 108]. The SEM photos of HgCdTe top (a) and cleaved (b) views after the dry etching of HgCdTe in inductively coupled plasma (ICP) [109] are shown in Fig. 15.9.

The advantage of dry etching technology is associated with anisotropic etching (see Fig. 15.9). The disadvantage of dry etching is the formation of a damaged layer on the surface after etching. Donor complexes are usually formed in the damaged layer. The formation of a donor complex in a damaged layer has been studied in detail during ion beam etching with argon [102, 103]. It was found that the donor complexes are based on interstitial Hg atoms captured by a defect formed during etching. In the damaged layer, the conductivity is converted from p- to n-type. The concentration of charge carriers over the thickness after ion etching of p-HgCdTe [111] is shown in Fig. 15.10. It is clear that the thickness of n-type conductivity at the

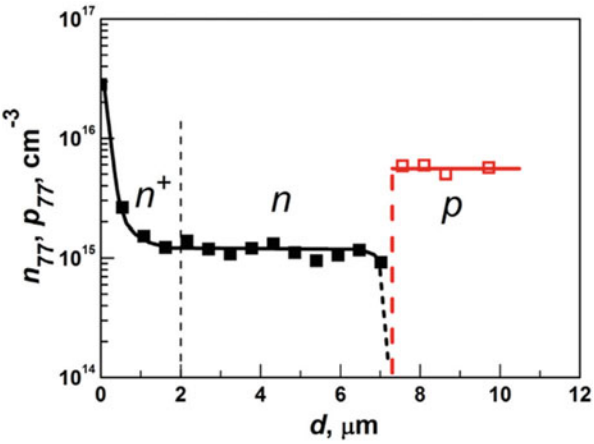

Fig. 15.10 The charge carrier concentration profile in ion-etched HgCdTe: solid squares corresponded to electrons, open squares corresponded to holes. (Reproduced with permission from Izhnin et al. [103]. Copyright 2017 Elsevier)

conversion process exceeds 7 μm. After dry etching of In-doped n-HgCdTe, a thin n +-type layer is formed on the surface. It should be noted that the concentration of electrons in the damaged layer depends on the storage time. Numerous studies showed that the thickness and electron concentration in the damaged layer depend on the ion energy, ion flux, and the temperature of etching. It was also found that the thickness of the damaged layer and etch depth are represented by the square root and linear dependences on time [112]. The Hg interstitial atom migration energy was determined as 120 ± 30 meV. To minimize the influence of the damaged layer on the characteristics of the diodes, it is proposed to remove the damaged layer by liquid etching followed by annealing [104].

The study [113] showed the possibility of plasma-chemical etching without the formation of a damaged layer. This method is very promising, since the technological process of removing the damaged layer formed during other dry etching processes is excluded.

15.4 HgCdTe Surface Passivation Technology

The HgCdTe surface passivation technology plays a key role in reducing or eliminating surface leakage currents. These currents lead to a significant increase in the dark current of photoconductor and photovoltaic detectors and a decrease in their sensitivity. The requirements for the HgCdTe surface passivation technology are the following [114, 115]:

- Good adhesion of the passivation layer
- Stability of the interface between the HgCdTe surface and the passivating layer during temperature cycling in the range of 78–300 K
- A small built-in charge

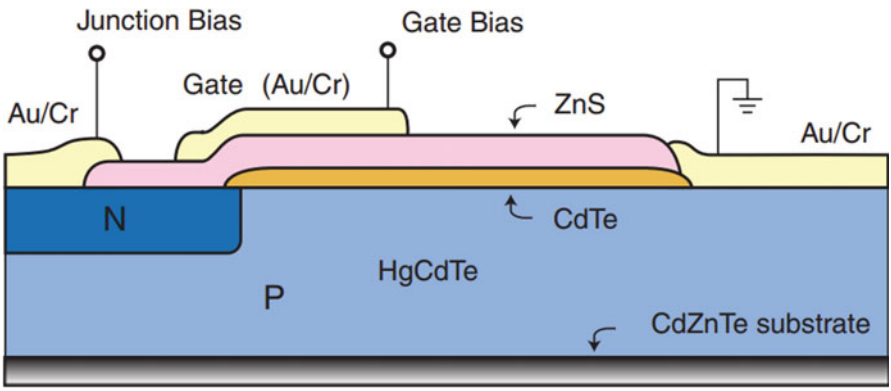

Fig. 15.11 The scheme of cross section of fabricated diodes on the base of Hg vacancy-doped p-type MWIR material from Fermionics Corporation grown by LPE. The CdTe is used as both a passivant and a mask for the plasma-based type conversion. The diodes were passivated with 200 nm of ZnS and contacts were formed with Au/Cr. (Reproduced with permission from Smith et. al., [110]. Copyright 2007 Springer)

The most developed passivation of the n-p diodes, fabricated on the basis of Hg vacancy-doped p-HgCdTe by CdTe and ZnS [115], is shown in Fig. 15.11.

The deposition temperature of the passivating layer is very important, since Hg begins to evaporate from the HgCdTe surface already at temperatures above 80 °C [116]. It should also be noted that for the passivation of p-HgCdTe, it is necessary to exclude the conversion of the conductivity type during the deposition of the passivation coating [117]. The built-in charge in the dielectric coating can significantly affect the quality of the photodiodes. It has been shown that the surface potential affects both the differential resistance diode (R_d) and the noise spectrum [115]. The noise spectrum of an n-p diode is shown in Fig. 15.12. It is clear that the noise is decreased with an increase of frequencies and depends on the gate voltage that should be explained by the influence of the built-in charge at the interface (passivation coating (CdTe+ZnS)/HgCdTe). It should be noted that there is a difficulty in identifying the density of surface states at the passivation coating/semiconductor interface. The most common Terman method for calculating the density of surface states requires an ideal capacitance-voltage (C-V) characteristic. The difficulties in the calculations of an ideal C-V characteristic are associated with the nonparabolicity of the HgCdTe band structure and the effects of quantization of charge carriers. The most complete consideration of all HgCdTe features when calculating the C-V characteristic was carried out in [118]. The authors used different approximations when calculating the ideal C-V characteristic. Therefore, it is impossible to statistically compare the density of surface states obtained in different studies.

The HgCdTe passivation technology can be conditionally divided into four types, taking into account the nature of coating layer, for example:

- Anodic and plasma oxides
- Sulfides

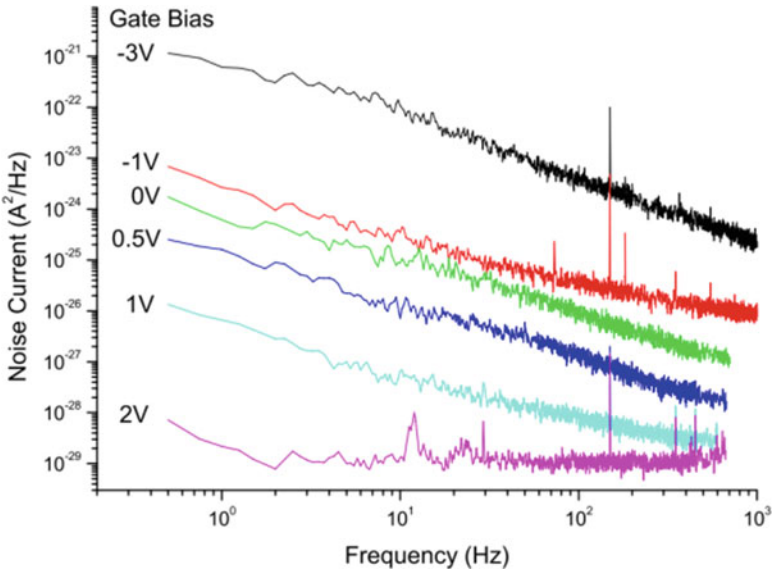

Fig. 15.12 The noise spectrum of a gated 300 μm in diameter photodiode at 77 K for various gate biases. (Reproduced with permission from Smith et. al., [110]. Copyright 2007 Springer)

- Deposited layers with dielectric properties (SiOx, SiNx, Al_2O_3)
- Wide bandgap semiconductors (HgCdTe, CdTe, ZnS)

Anodic oxide (AO) effectively passivates the surface of n-HgCdTe and therefore can be used in the manufacture of IR photoconductive detectors. Wet anodizing is carried out at room temperature in a solution of 0.1 M KOH in 90% ethylene glycol/10% water at a current density of 0.1–0.3 mA·cm^{-2} [119]. However, upon passivation of p-HgCdTe with anodic oxide, a large positive fixed charge is formed on the surface of the n-type inversion layer. The density of fixed anodic oxide/HgCdTe surface charge varies within (5–20) × 10^{11} cm^{-2}. The fast surface states are U-shaped and have a minimum located at the center of bandgap. Slow surface traps cause small hysteresis in the C-V characteristics. Therefore, the anodic oxide is not used as a passivation coating for the HgCdTe surface in the manufacture of IR photodetectors [117].

Plasma oxides also have passivating properties. They are grown on the HgCdTe surface using a commercial gas mixture of oxygen and trifluoroethane in a commercially available plasma stripper system (LFE Corporation, model PDS/PDE-301). Low-pressure cold oxygen plasma (0.2–0.4 Torr) is formed by RF power supply (10–50 W, 13.5 MHz). The HgCdTe sample has a positively biased voltage (20–100 V) relative to ground. The fixed surface charge (plasma oxide)/HgCdTe interface is 1 × 10^{11} cm^{-2} which is an order of magnitude lower than in the case of anodic oxide. The fast surface states are located at the center of bandgap with a minimum of 2 × 10^{11} cm^{-2}eV^{-1}. The absence of hysteresis in the C-V characteristics indicates the absence of slow traps. Plasma oxides have shown excellent

thermal stability. The flat band structure and fixed surface charge density are constant up to 90–95 °C. Nemirovsky and Bakhir [119] believe that this effect is probably due to the presence of fluorine in the oxide.

Anodic sulfides are very stable compounds. However, in several cases, anodic sulfides dissolve preferably in polysulfide solutions with an appropriate pH. The technological process of obtaining CdS on the HgCdTe surface by the anodic method was shown in [120]. Anodic sulfide films were grown in an electrochemical cell with a carbon counter electrode without using aqueous basic sulfide solutions in ethylene glycol at current density of 60–140 $\mu A \cdot cm^{-2}$ and growth rate of ~10 A/min. The stable state of native sulfides on the $Hg_{0.78}Cd_{0.22}Te$ surface was shown at the thermal surface heating in vacuum up to 95 °C [121].

The excellent surface passivating properties of the silicon oxide could not be maintained during prolonged heating of the device in a vacuum [1]. In addition, there are problems with SiO_2 layer adhesion [121]. It is interesting to note that the best results are obtained with SiO_2 when several layers of native or anodic oxide are present on the HgCdTe surface before the deposition of SiO_2. An extremely thin native oxide (5–10 nm) protects the crystal from damage and possibly improves the adhesion of the SiO_2 layer [122]. The passivation properties of $SiO_2/Hg_{0.7}Cd_{0.3}Te$ interface were studied in [123]. Interfacial trap density (D_{it}) was evaluated by measuring the difference between high- and low-frequency C-V curves [124]. The surface-state densities (4–5) × 10^{11} cm^{-2} eV^{-1} in the bandgap center and (2–4) × 10^{13} cm^{-2} eV^{-1} near the valence band were found. The density built-in charge was 10^{10} cm^{-2}.

The ZnS antireflection coating for HgCdTe photoconductors has been used with varying success and was not stable during vacuum baking [1, 125]. The properties of $ZnS/Hg_{0.8}Cd_{0.2}Te$ interface were investigated by measuring the C-V characteristics of MIS structures [126]. The density of surface states in the range (1–6) × 10^{11} cm^{-2} eV^{-1} was obtained by measuring the C-V characteristics at a frequency of 1 MHz in the parabolic band approximation using the formulas given in [127]. ZnS thin films were prepared by vacuum evaporation using conventional evaporation systems from a quartz boat slowly heated in a resistance furnace or with an electron gun.

The SiN_x layers were robust and chemically resistant with good passivation quality and thermal stability. In [128] the authors described the SiN_x layer deposition in ICPECVD system with $SiH_4 + N_2$ gas mixtures in the temperature range of 80–100 °C. The interface trap density (D_{it}) was determined by the C-V measurement at 1 kHz and 1 MHz using MIS structure on $Hg_{0.68}Cd_{0.32}Te$ [129]. The minimum density of fast traps D_{it} was 4 × 10^{10} cm^{-2} eV^{-1}.

The good passivation properties of the Al_2O_3 layer grown by the plasma-enhanced ALD (PEALD) method on the HgCdTe surface were demonstrated in [118, 130, 131]. The trimethylaluminum (TMA) was as a source of Al. Oxygen plasma plays the role of an oxidizing agent. The Al_2O_3 coating layers were deposited on side surfaces of mesa structures [132]. In addition, it was shown that the lifetime of minority carriers in HgCdTe increased after ALD deposition at room temperature [132]. It has been found that the optimal Al_2O_3 deposition is observed in the range

120–160 °C [130]. Wide-gap II-VI compounds were also studied as a surface passivation coating for HgCdTe. CdTe is now considered the most advantageous material for this purpose due to its high resistivity and crystal lattice close to that of HgCdTe [133–135]. CdTe is chemically stable, more robust than HgCdTe, and transparent to IR radiation. As a result, CdTe has become the most important and widely used passivation coating in HgCdTe technology for the production of IR photoelectric detectors [136]. The deposition of a CdTe layer on the HgCdTe surface requires a low temperature to prevent mercury depletion. Kumar et al. [135] compared the passivating properties of CdTe and AO deposited on the n-n-$Hg_{0.786}Cd_{0.214}Te$ surface. A 100 nm in thickness CdTe layer was deposited using thermal evaporation. The n-HgCdTe surface passivated with CdTe had a surface recombination rate approximately five times lower than the AO-passivated surface. The activation energy of the surface trap for CdTe- and AO-passivated HgCdTe surface, estimated from the data analysis, was in the range of 6–8 meV. This trap level is associated with Hg vacancies at the HgCdTe surface. The fixed charge density for the CdTe/HgCdTe interface measured by the C-V method was (5–9) × 10^{10} cm^{-2}.

15.5 Electric Contact Technology

Metal contacts to semiconductors play a key role in the manufacture of the device, affecting its long-term performance and reliability. The basic characteristics of metallic contacts are contact resistance value, recombination at the interface with the contact, 1/f noise, and long-term and thermal stability [137, 138]. Ideal ohmic contacts are obtained when the work function of the metal is less than the electron affinity of the n-type semiconductor. However, the surface properties of II-VI semiconductors are often poorly understood. Therefore, in practice, ohmic contacts are usually made according to empirical recipes. In this regard, in order to reduce the influence of the surface on the contact resistance, a heavily doped region is often formed on the surface. In this case, the thickness of space charge region is greatly reduced, allowing the electrons to tunnel, resulting in a low resistance. As a rule, contacts consist of several layers of various metals, which are necessary to improve adhesion and reduce solid-state reactions.

In Ref. [139] it is performed a theoretical analysis of the position of the Fermi level at the metal/$Hg_{1-x}Cd_xTe$ interface. For extrapolation from CdTe to $Hg_{1-x}Cd_xTe$, three models of the pinning of the Fermi level at the metal-semiconductor interface were used [140]. Two models of Schottky barrier pinning were considered: Spicer defect model [141, 142] and the metal-induced gap-state model (MIGS) [143]), as well as the third model based on the effective work function [144]. The consideration of these models gives the same overall result showing the formation of ohmic contacts to n-type HgCdTe with a composition less than a certain value and nonohmic-rectifying contacts to all p-type HgCdTe. Results of these considerations are shown in Fig. 15.13. These results show that ohmic

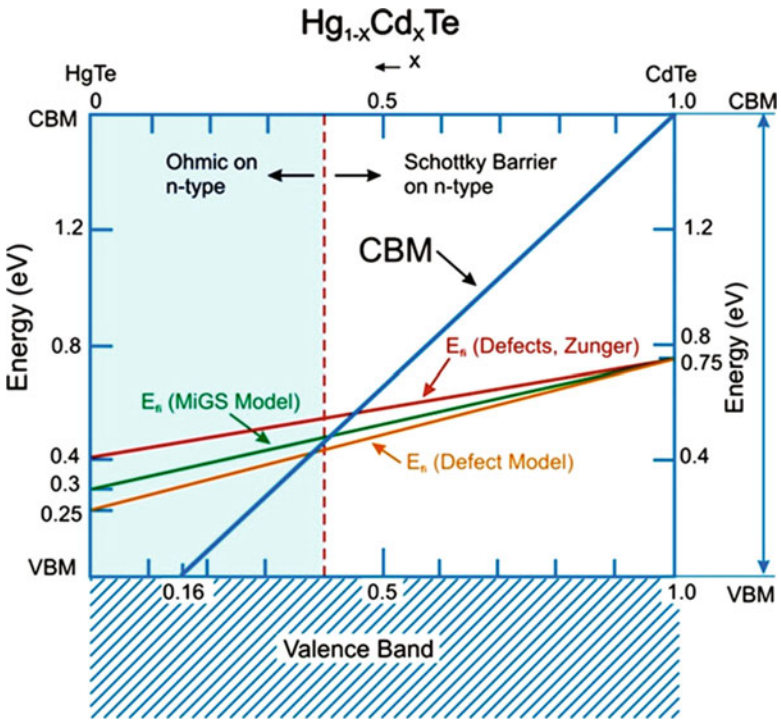

Fig. 15.13 The energy of Fermi-level position (E_{fi}) at the interface on HgCdTe composition. For this extrapolation, two models (MIGS and defects) were used. Near x = 0.4, E_{fi} moves into the conduction band, providing its own ohmic contacts on the n-type material. (Data extracted from Freeouf et al. [144])

contacts are to be expected to n-type HgCdTe at $x < 0.4$, in contrast to p-type HgCdTe where a Schottky barrier should form regardless of composition.

The most commonly used metal for n-$Hg_{1-x}Cd_xTe$ is indium [145–147], which has a low work function. Leech and Reeves investigated In/n-HgCdTe contacts, which exhibited an ohmic nature in the composition range x = 0.30–0.68 [148]. The charge carrier transport in these contacts was attributed to the process of field effect thermal emission. This behavior was explained by the formation of the n^+-region under the contact upon rapid diffusion of In, which is a donor impurity in HgCdTe. The specific contact resistance ranged from 2.6×10^{-5} ohm cm^2 at x = 0.68 to 2.0×10^{-5} ohm cm^2 at x = 0.30, which correlates with the change in the resistivity of the HgCdTe layer. In the general case, an ohmic contact with p-type HgCdTe is more difficult to implement, since a large work function of the contact metal is required. Au, Cr/Au, and Ti/Au were most commonly used for p-type HgCdTe. Beck et al. [149] showed that Au and Al contacts with p-type $Hg_{0.79}Cd_{0.21}Te$ are ohmic with specific contact resistance from 9×10^{-4} to 3×10^{-4} Ω cm^2 at room temperature. The dependences of the 1/f noise implied that the noise in the Au contact originated

at the Au/HgCdTe interface or near it, while the noise in the Al contacts originated from the surface conduction layer near the contact.

The metal contacts of Pt, Cu, and Au with p-HgCdTe were studied in [150]. For this purpose, depth profiles were measured using SNMS, SIMS, AES, and XPS methods. I-V characteristics were measured and then compared with both the distribution profile of metal concentration throughout the thickness of interface and chemical state at the metal/HgCdTe interface. It was found that Pt does not form an ohmic contact with HgCdTe, while Cu forms unstable ohmic contacts. Au forms ohmic contacts by diffusion at elevated temperatures and exhibit long-term stability. Therefore, Au is currently the preferred metal for making ohmic contacts to p-HgCdTe. In [151], the authors proposed a method for manufacturing ohmic contacts to n- and p-type HgCdTe layers in a single technological cycle. The ohmic behavior of Cr, Mo, and Ti with HgCdTe ($x \approx 0.3$) does not depend on the metal used for both n- and p-type MCT layers and indicates that the Fermi level is pinned. The ohmic or close to ohmic behavior of Cr, Mo, and Ti contacts can be explained by the reactive nature of metals. The contact resistance R_c is significantly less than the resistance of the p-n junction HgCdTe ($x \approx 0.3$) R_0 at zero bias at 80 K ($R_cA < 10^{-2}$ ohm cm^2 and $R_0A > 10^3$ ohm cm^2, where A is p-n junction area). Thus, such contacts are suitable for manufacturing HgCdTe photovoltaic detectors. Cr, Mo, and Ti were chosen for the deposition at room temperature, since, as a rule, they provide a high adhesion to HgCdTe layers. Au and In were used as bonding spacers to which gold contact wires were attached by ultrasonic welding or micro-soldering. It was shown that under the used deposition conditions, gold has low adhesion to HgCdTe epitaxial layers. However, for light-doped p-type $Hg_{1-x}Cd_xTe$, there are no good contacts, and all metals tend to form Schottky barriers. This problem is especially difficult for HgCdTe with a high HgCdTe composition. This problem can be solved by using a highly doped region near the metal contact to increase the tunneling current. However, in practice, it is difficult to achieve the required high p-type doping. One of the practical solutions is the use of HgCdTe growth with a narrowing bandgap at the metal/HgCdTe interface [152]. An analogous decision was used for manufacturing the ohmic contact to CdTe and for the $Cd_{0,7}Hg_{0,3}Te$ p-type conductivity [153]. It was proposed to use HgTe, the work function of the metal contact which corresponds to p-CdTe. The HgTe contacts were deposited by the vapor-phase epitaxy on a CdTe surface etched in Br_2/methanol (CH_30H). The interdiffusion zone formed a graded junction between the bandgaps of HgTe and CdTe without rectifying. This allows suppression of barrier at interface. The CdTe/HgTe/Au energy band diagram is shown in Fig. 15.14.

The measured specific contact resistances are ten times lower than the best results obtained so far.

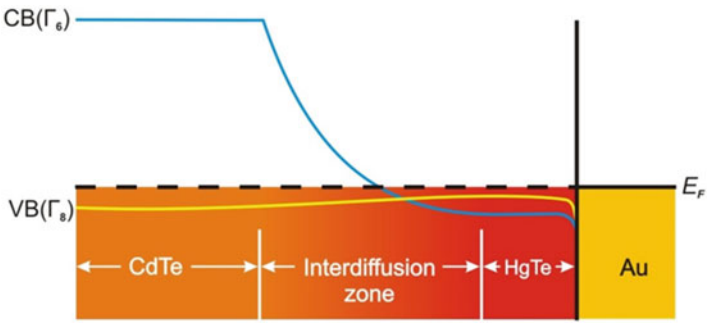

Fig. 15.14 The equilibrium energy band diagram at room temperature in CdTe/HgTe/Au: *CB* conduction band, *VB* valence band. (Data extracted from Janik et al. [153])

15.6 p-n Junction Technology

The p-n junction in HgCdTe is formed by numerous methods, including in and out diffusion of Hg and impurity diffusion, ion implantation, electron bombardment-induced conduction, plasma-induced-type transformation, and doping during growth from the vapor or liquid phase [5, 117, 154–156]. A brief description of the main methods of p-n junction formation in HgCdTe layers is presented in [138]. Low binding energies of ionic bonds in HgCdTe influenced the technological processes of the formation of p-n-junctions. Free Hg atoms were formed in the processes of ion implantation and ion beam etching. This creates much deeper transitions than it would be expected only from ion implantation. The dislocations play a certain role in the elimination of Hg vacancies. The role of Hg, impurities, dislocations, and ion implantation in the formation of p-n junction is very complex and insufficiently studied. Nevertheless, producers have obtained a good phenomenological control of the transition depths and dopant profile through various p-n junction formation processes. Recently, the epitaxial methods with doping in the growth process have been used to obtain p-n junctions. MBE and MOCVD were successfully implemented by doping with In and As during growth, as shown earlier (see Sect. 15.2.2).

15.6.1 Mercury Diffusion

It is relatively easy to achieve the conversion of p-HgCdTe to the n-type due to vacancy annihilation during free diffusion of Hg atoms. The n-type conductivity layer is determined by the background donor impurity. Dutton et al. [157] summarized the knowledge about the mercury diffusion process. The mercury diffusion accompanied with the vacancy diffusion created the p-n junction at 200–250 °C in p-HgCdTe ($p \sim 10^{16}$ cm^{-3}) in 10–15 min. This corresponds to a diffusion coefficient

$\sim 10^{-10}$ $cm^2 s^{-1}$. The presence of dislocations can increase the mobility of vacancies. The presence of Te precipitates can decrease the Hg motion in the lattice. Jenner and Blackman reported about the free Hg diffusion from the AO [158]. Anodic oxidation results in the formation of a mercury-rich layer at the interface. Hg diffuses into the substrate during the thermal annealing resulting in the formation of an n-type HgCdTe. In addition, the anodic oxide layer acts as a diffusion mask to prevent the loss of mercury in vacuum upon contact with the surrounding atmosphere. This method is especially suitable for high-speed devices where the low and uniform doping of n-type regions is required.

15.6.2 Ion Etching

The low-energy ion bombardment is used to fabricate p-n junctions by conversion of the vacancies doped with p-HgCdTe into n-type [159, 160]. The ion beam introduces a small fraction of free Hg atoms (approximately 0.02% of ion gas atoms) into the lattice. Then Hg atoms fill Hg vacancies, creating weakly doped n-type background atoms, limited by donor atoms. The ion energy and dose are usually less than 1 keV and range from 10^{16} to 10^{19} cm^{-2}, respectively. Blackman showed that the p-n junction depth depends on the ion dose and can extend for several hundred microns from the surface [159]. The Hg diffusion during ion etching is very fast, even in comparison with experiments on thermal annealing of HgCdTe at 500 °C. The deeper p-n junctions are created by using higher ion beam current, longer etching time, lower beam voltage, and higher ion mass. The whole process is carried out at low temperatures that do not change the initial HgCdTe electrophysical properties and the quality of passivation. The p-type material conversion using an ion beam have been commercially used by GEC-Marconi Infrared Ltd. for FPAs based on HgCdTe since the late 1970s [161].

15.6.3 Reactive Ion Etching

Reactive ion etching is a method of reactive chemical plasma etching of a substrate surface, often used in microelectronics to remove material from a surface. Plasma is created at low discharge gas pressure. Ions are accelerated by the applied voltage between the plasma and the substrate. The combined physical processes involve ion sputtering and chemical reactions on the surface, resulting in the formation of volatiles and their desorption. This plasma-induced method is also used as a technology for the formation of p-n junctions [99, 162]. It is important to note that if postimplantation thermal annealing is required when using ion implantation to create p-n junctions in the process of manufacturing high-quality photodiodes, then when

reactive ion etching is used for these purposes, such annealing is not required. The conductivity conversion of p-HgCdTe in reactive ion etching technology occurs due to the formation of a source of free Hg atoms. Hg atoms quickly diffuse into the bulk of HgCdTe, decreasing the concentration of Hg vacancies occupying their crystal lattice points. Residual donor impurities become dominant in conductivity and participate in the formation of p-n junctions.

15.6.4 Ion Implantation

The ion implantation in HgCdTe is a widely and well-proven technology applied to fabricate photovoltaic HgCdTe FPAs [163–167]. N^+-p junctions are formed by the implantation of Al, Be, In, and B ions into the vacancy-doped p-type HgCdTe material. Usually, the ion implantation technology uses light ions, such as B or Be, to form the n-region. The ion flux with doses 10^{12}–10^{15} cm^{-2} and an energy range of 30–200 keV are usually used. Regardless of the nature of the ion atoms used, the n-type layer is associated with a material damage, as Voith first noted [168]. In the case of the ion implantation in p-type or n-type HgCdTe, the junction has N^+-p or N^+-n-p types. The N^+-n-p junction is the most desirable case because it is located far from the region of radiation defects. It is not necessary to use postimplantation thermal annealing to achieve high performance of SWIR and MWIR devices, especially at lower ion doses during implantation. However, many researchers have now concluded that the photodiode characteristics can be improved by the thermal annealing after ion implantation to eliminate radiation damages [169]. The annealing temperature depends on the nature of the ions and the conditions of the implantation process. At low radiation fluxes, the dark current noise can lead to a deterioration in the parameters of the diode. In this case, deliberate doping of the p-type absorber layer can be used to make n-p diodes. This makes it possible to increase the parameter R_0A by almost an order of magnitude for long-wavelength IR FPAs with a cutoff wavelength up to 20 μm [170].

The main trend and the most promising direction in the development of research and technology is the creation of photovoltaic IR FPAs based on the P^+-n junction [171, 172]. The motivation for the study is associated with the expansion of the spectral range of sensitivity in the long-wavelength region of 8–14 microns and/or operating at elevated temperatures. Au, Ag, Cu, and P ions were used as implants to convert n-type HgCdTe with a subsequent thermal annealing. As a rule, p-n junctions are located in a depth of 1–3 μm from the HgCdTe surface, which is significantly larger than the area of implanted ions less than 30 nm [173]. Based on long-term studies of the technology of ion implantation with various chemical elements, As was chosen as the only impurity, which showed the high-quality p-on-n-type IR FPA detectors and determined the main development for industrial production. To create the P^+-n junction, In and As are used as base donor and acceptor impurities, respectively. The main problem is associated with the need to carry out the As activation using thermal annealing at high temperatures (more than 300 °C), which

creates great problems for further technological processes. However, the design of the P+-n-type photodiode can significantly reduce the dark current and the resistance spreading over the base layer due to long-living minority carriers (holes) and highly mobile majority carriers (electrons), respectively. Nowadays, many companies conduct intensive research and development of IR FPAs based on the P+-n junction technology using HgCdTe HES grown by LPE, MOCVD, and promising MBE [174–177].

15.6.5 p-on-n Versus n-on-p HgCdTe Diodes

Among the technologies for the formation of p-n junctions, the most widely used methods are the ion implantation and doping during growth [178]. The doping-during-growth method is mainly used to create multispectral IR FPAs, using mesa etching technology. Ion implantation methods are used to create both single-color and multicolor IR FPAs, created by planar and mesa topologies, respectively [179]. A photograph of a pseudoplanar topology of 256 × 256 dual-band IR FPAs fabricated using ion implantation technology to form n-p junctions in the wide-gap (MWIR) and narrow-gap (LWIR) HgCdTe layers is shown in Fig. 15.15 [179].

Dark current is the fundamental parameter of a photon photodiode and is determined by the thermal charge carrier generation [180]. The generated thermal dark current is calculated on the basis of the following expression $G_{th} = n_{maj}/2\alpha\tau_{Ai}$, where G_{th} is thermal generation rate, n_{maj} is concentration of the majority carriers, α is absorption coefficient, and τ_{Ai} is Auger lifetime of minority carriers. In n-HgCdTe layers, the minority carrier lifetime is determined by the Auger 1 process, including two electrons and a heavy hole. Thermally generated normalized dark current density for MWIR and LWIR, based on n-HgCdTe for two cutoff wavelengths of 5 μm and 10 μm, and the background flux for F/2 optics are shown in Fig. 15.16. The

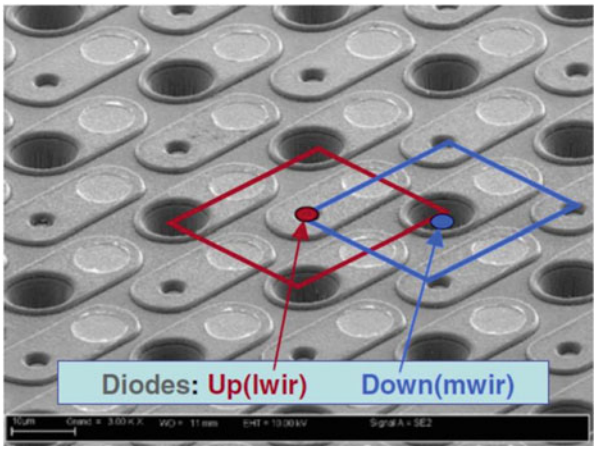

Fig. 15.15 The top and cross-section view of scheme (up) and photo (down) two-color 256 × 256 MWIR and LWIR IR FPA. (Reproduced with permission from Destefanis et al. [179]. Copyright 2007 Springer)

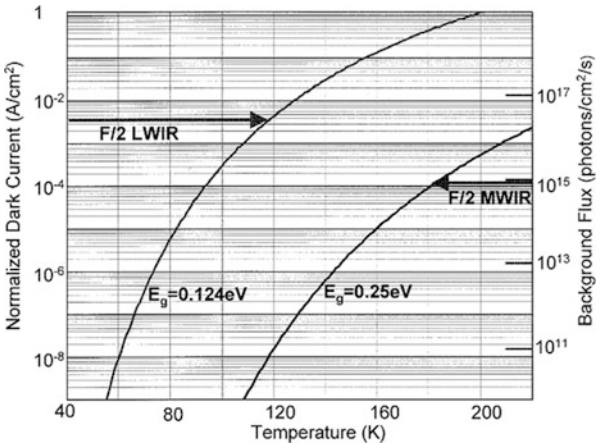

Fig. 15.16 The normalized dark current density vs. temperature for MWIR and LWIR based on n-HgCdTe. (Reproduced with permission from Kinch [180]. Copyright 2000 Springer)

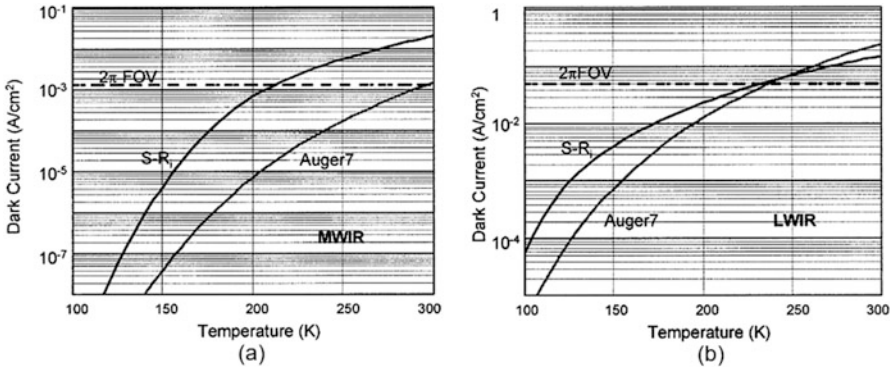

Fig. 15.17 Shockley-Read (S-R) and Auger 7 dark current vs. temperature for P^+-π-N^+ HOT MWIR (**a**) and LWIR (**b**) detector with Na = 5×10^{14} cm^{-3}. (Reproduced with permission from Kinch [180]. Copyright 2000 Springer)

electron concentration and the layer thickness were 10^{15} cm^{-3} and 10 μm (~1/α), respectively. It is clear that BLIP regime can be reached at temperatures <120 K for LWIR and at <180 K for MWIR. The similar representation of thermal dark current should be used for a p-type material, taking into account the Auger 7 recombination mechanism, including two heavy holes and one electron, as shown in [181]. The minority lifetime τ_{Ai7} in p-HgCdTe is longer than in n-HgCdTe ($\tau_{Ai7} = (6–20)\,\tau_{Ai1}$). It means that the thermally generated dark current in the p-HgCdTe layers will be 6–20 times less than in the n-HgCdTe layer. The calculations of dark current, limited by Auger and S-R carrier recombination for the HgCdTe HOT IR detector (P+-ν-N + architecture), made by Kinch [180] for the p-HgCdTe layer with a low acceptor concentration in Na = 5×10^{14} cm^{-3}, are shown in Fig. 15.17.

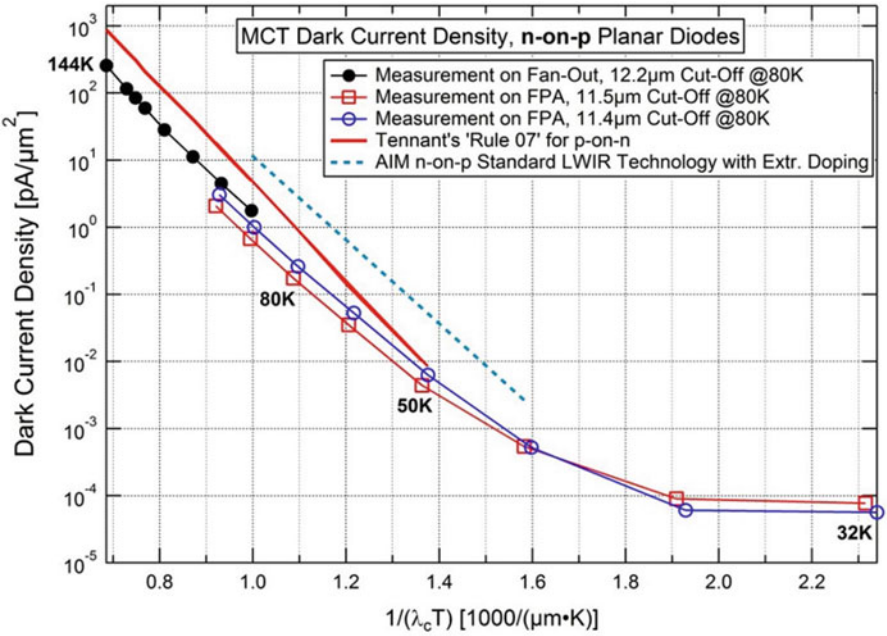

Fig. 15.18 Thermal dark current density versus detector operating temperature for p-on-n (a) and n-on-p LWIR and VLWIR HgCdTe detectors with cutoff wavelengths at 80 K (see in insert). (Reproduced with permission from Hanna et al. [184]. Copyright 2016 Springer)

It is clear that in the case of Auger carrier recombination, it is possible to achieve operation with the background-limited performance (BLIP) for MWIR detectors at room temperature. In the case of LWIR detectors, BLIP operation is possible at temperature up to 220–230 K.

Usually, for n-on-p-type HgCdTe detectors, p-type absorber layer is doped with Hg vacancies with a concentration of ~10^{16} cm^{-3}. In this case, the dark current of IR detectors (intrinsic) is being determined by S-R center parameters. The essential improvement of the photovoltaic characteristics of IR detectors is achieved by doping the absorber layer with intentional acceptor impurities.

Doping of the HgCdTe absorber layer with Au to a hole concentration of $<5 \times 10^{15}$ cm^{-3} was made in AIM (https://www.aim-ir.com/de/home.html) [182, 183]. A comparison of the characteristics of p-on-n and n-on-p LWIR and VLWIR detectors, manufactured by AIM technology, is presented in [184]. P-n junctions were formed by ion implantation of As and B into n-type and p-type absorbing layers doped with In and Au, respectively. The HgCdTe absorber layers were grown by LPE on CdZnTe substrates. The temperature dependences of the dark current density for LWIR and VLWIR FPAs and photodiodes for the n-on-p technology with cutoff wavelengths 11.4 μm, 11.5 μm, and 12.2 μm, measured at 80 K, are shown in Fig. 15.18. For comparison, the dependences according to Tennant's Rule 07 for p-on-n diodes and for AIM n-on-p diodes on HgCdTe layers

doped with external impurities according to the standard LWIR technology are also shown in this figure. It is clear that the fabrication of an IR FPA with an n-on-p junction based on p-HgCdTe doped with intentional impurity (Au in AIM) shows results comparable to those obtained for the p-on-n junction, providing the operation of IR FPA in the background-limited (BLIP) mode at elevated temperatures. This opens up a new trend in the development of SWaP (size, weight, and power) technology of IR detector.

15.7 Conclusion

Since the 1960s, HgCdTe device technology has been developed in many countries. Most of the research has focused on infrared detectors and focal plane arrays, mainly operating in photoconduction or photovoltaic modes. Due to its unique physical properties, the solid solution compounds of HgCdTe alloys have taken a leading position among light-sensitive IR materials and made it possible to fabricate IR FPAs that are sensitive in a wide spectral range and, first of all, in "atmospheric windows." The technologies of HgCdTe materials, starting from a bulk crystal, have gone through the development of epitaxial growth by various methods. The simplest LPE technique ensured the development of technology on CdZnTe substrates and reached the modern level as an industrial technology for obtaining very high-quality HgCdTe epilayers. The existing limitations in the properties of CdZnTe substrates, difficulties of their preparing, and, finally, their high cost lead to the development of vapor-phase epitaxy on a large-diameter GaAs and Si substrate by MOCVD and MBE technologies. Now MOCVD technology provides high-quality HgCdTe on GaAs substrate. MBE is a very flexible technology which allows growing both HgCdTe hetero- and nanostructures with a high-accuracy control of the composition and thickness of the layer at the nanometer level. Currently, MBE HgCdTe technology on large substrates provides a high-quality, inexpensive photosensitive material for large-format IR FPAs. It is shown that MBE HgCdTe/Si HES provides the possibility of industrial production of IR detectors for SWIR and MWIR spectral ranges. The study of etching mesotechnology showed that dry etching has practically no effect on the size of pixels when they are separated even at great depths, which is required in the manufacture of large-format IR MFPs. Passivation technology is necessary to protect the pixel surface and prevent the appearance of leakage current. The best passivation materials are CdTe and/or dielectric layers. The conducted study of electrical contacts identified metals such as In and Au, which provide ohmic contacts with the n-type and p-type HgCdTe material. The considered versions of p-n junction technologies show that the p-on-n type formed by the implantation of As ions into an n-HgCdTe absorber or growing DLHJ gives a significant decrease in the dark current. The developed n-on-p type based on intentional doping of the p-HgCdTe absorber with acceptor impurities has parameters similar to the p-on-n type. These two types provide the ability to operate IR detectors at elevated temperatures, which allows the development of SWaP technologies.

References

1. Norton P (2002) HgCdTe infrared detectors. Opto-Electron Rev 10(3):159–174
2. Rogalski A, Antoszewski J, Faraone L (2009) Third-generation infrared photodetector arrays. J Appl Phys 105:091101. https://doi.org/10.1063/1.3099572
3. Lawson WD, Nielsen S, Putley EH, Young AS (1959) Preparation and properties of HgTe and mixed crystals of HgTe-CdTe. J Phys Chem Solids 9:325–329
4. Shneider AD, Gavrishchak IV (1960) The structure and properties HgTe-CdTe. Phisica Tverdogo Tela 2:2079–2081. (in Russian)
5. Capper P, Garland J (eds) (2011) Mercury cadmium telluride. Growth, properties and applications. Wiley, Chichester, p 556
6. Capper P (ed) (1994) Properties of narrow gap cadmium-based compounds. IEE, INSPEC, London, p 620
7. Capper P (1994) The role of accelerated crucible rotation on the growth of HgCdTe and CdTe/CdZnTe. Prog Cryst Growth Charact 28(1–2):1–55. https://doi.org/10.1016/0960-6974(94)90012-4
8. Capper P (2017) A UK retrospective- reminiscence of crystal grower. J Electron Mater 46(9):5430–5441. https://doi.org/10.1007/s11664-0175563-0
9. Tregilgas JH (1994) Development of recrystallized bulk HgCdTe. Prog Cryst Growth Charact 28(1–2):57–83. https://doi.org/10.1016/0960-6974(94)90013-2
10. Triboulet R (1994) The Traveling Heater Method (THM) for HgCdTe and related materials. Prog Cryst Growth Charact 28(1–2):85–144. https://doi.org/10.1016/0960-6974(94)90014-0
11. Ponomarenko VP (2003) Cadmium mercury telluride and the new generation of photoelectronic devices. Physics-Uspekhi 46(6):629–635. https://doi.org/10.1070/PU2003v046n06ABEH001372
12. Bogoboyashchiy VV, Kurbanov KR, Oksanich AP (2000) Industrial production of GaAs and $Hg_{1-x}Cd_xTe$ based crystals and epitaxial structures in Ukraine: actuality and development outlook. Funct Mater 7(3):546–551
13. Castro CA, Tregilgas JN (1988) Recent developments in HgCdTe and HgZnTe growth from Te solution. J Cryst Growth 86:138–145. https://doi.org/10.1016/0022-0248(90)90711-S
14. Astles M, Blackmore G, Steward V, Rodway DC, Kirton P (1987) The use of in-situ wash melts in the LPE growth of (CdHg)Te. J Cryst Growth 80:1–8. https://doi.org/10.1016/0022-0248(87)90516-1
15. Radhakrishnan LK, Sitharaman S, Gupta SC (2003) Liquid phase epitaxial growth of HgCdTe using a modified horizontal slider. J Cryst Growth 252(1–30):79–86. https://doi.org/10.1016/S0022-0248(02)02530-7
16. Parker SG, Weirauch DF, Chandra D (1988) Terracing in HgCdTe LPE films grown from Te solution. J Cryst Growth 86(1–4):173–182. https://doi.org/10.1016/0022-0248(90)90714-V
17. Edwall DD, Gertner ER, Tennant WE (1984) Liquid phase epitaxial growth of large area $Hg_{1-x}Cd_xTe$ epitaxial layers. J Appl Phys 55(6):1453–1460. https://doi.org/10.1063/1.333400
18. Gupta SC, Sitharaman S, Nagpal A, Gautam M, Berlouis LEA (1996) Growth and characterization $Hg_{1-x}Cd_xTe$ ($0.21<x<0.36$) epilayers grown from Te – rich solution by the dipping technique. J Cryst Growth 165(1–2):19–24. https://doi.org/10.1016/0022-0248(95)00993-0
19. Bowers JE, Schmit JL (1982) Mercury containment for liquid phase growth of mercury cadmium telluride from tellurium-rich solution. US Patent 4,317,689, 2 March 1982
20. Hager RJ (1987) Wipe-off apparatus of liquid phase epitaxy of mercury cadmium telluride. US Patent. 4,706,604, 17 Nov., 1987
21. Biao L, Chen XQ, Chu JH, Cao JY, Zhu JQ, Tang DY (1996) Growth and characterization of liquid – phase epitaxial $Hg_{1-x}Cd_xTe$ films. Thin Solid Films 278:1–5. https://doi.org/10.1016/0040-6090(95)08122-4
22. Tung T (1988) Infinite – melt vertical liquid – phase epitaxy of HgCdTe from Hg solution: status and prospects. J Cryst Growth 86(1–4):161–172. https://doi.org/10.1016/0022-0248(90)90713-U

23. Colombo L, Westphal GH, Liao PK, Chen VC, Schaake HF (1992) Producibility of (Hg,Cd) Te by dipping liquid phase epitaxy. Proc SPIE 1683:33–39. https://doi.org/10.1117/12.137777
24. Kalisher MH (1984) The behavior of doped $Hg_{1-x}Cd_xTe$ epitaxial layers grown from Hg-rich melts. J Cryst Growth 70(1–2):365–372. https://doi.org/10.1016/0022-0248(84)90288-4
25. Tung T, DeArmoud LV, Herald RF, Herning PE, Kalisher MH, Olson DA et al (1992) State of the art of Hg – melt LPE HgCdTe at Santa Barbara research center. Proc SPIE 1735:109–134. https://doi.org/10.1117/12.138616
26. Sangha SPS, Medland JD, Berry JA, Rinn LM (1987) Low temperature epitaxial growth of cadmium telluride from mercury solvent. J Cryst Growth 83(1):127–136. https://doi.org/10.1016/0022-0248(87)90513-6
27. Yoshikawa M, Ueda S, Takigawa H (1985) High – purity HgCdTe with low dislocation density, grown by LPE. Fujitsu Sci Tech J 25(5):494–503
28. Janik E, Ferah M, Legros R, Triboulet R, Brossat T, Riant Y (1985) LPE growth and characterization of 1.3 μm (Hg,Cd)Te layers. J Cryst Growth 72(1–2):133–138. https://doi.org/10.1016/0022-0248(85)90131-9
29. Sydorchuk P, Khlyap G, Andrukhiv A (2001) Growth and some properties of heterostructures based on new narrow-gap semiconductor ZnCdHgTe. Cryst Res Technol 36(4–5):361–369. https://doi.org/10.1002/1521-4079(200106)36:4/53.0.CO;2-5
30. Ruda H, Jedral L, Lagowski J, Gatos HC (1984) Mercury – pressure – induced epitaxy of HgCdTe. J Electrochem Soc 131(5):1159–1163. https://doi.org/10.1149/1.2115770
31. Belogorokhov AI, Denisov IA, Smirnova NA, Belogorokhova LI (2004) The investigation of structural perfection of CdHgTe/CdZnTe epitaxial layers by Raman scattering method. Semiconductors 38(1):82–90. https://doi.org/10.1134/1.1641138
32. Li B, Chu JH, Zhu JQ, Chen XQ, Cao JY, Tang DY (1996) Growth of $Hg_{1-x}Cd_xTe$ liquid phase epitaxial films on vicinal planes. J Cryst Growth 169:480–484. https://doi.org/10.1016/0022-0248(96)00418-6
33. Takigawa H, Yoshikawa M, Maekawa T (1988) Dislocation in HgCdTe – CdTe and HgCdTe – CdZnTe heterojunction. J Cryst Growth 86(1–4):446–451. https://doi.org/10.1016/0022-0248(90)90757-C
34. Yoshikawa M, Maruyama K, Saito T, Maekawa T, Takigawa H (1987) Dislocation in HgCdTe/CdTe and HgCdTe/CdZnTe heterojunctions. J Vac Sci Technol A 5(5):3052–3054. https://doi.org/10.1116/1.574214
35. Vydyanath HR (1996) Incorporation of dopants and native defects in bulk $Hg_{1-x}Cd_xTe$ crystals and epitaxial layers. J Cryst Growth 161(1–4):64–72. https://doi.org/10.1016/0022-0248(95)00613-3
36. Vydyanath HR (1981) Lattice defects in semiconducting $Hg_{1-x}Cd_xTe$ alloys. I. Defect structure of undoped and copper doped $Hg_{0.8}Cd_{0.2}Te$. J Electrochem Soc 128(12):2609–2619. https://doi.org/10.1149/1.2127314
37. Vydyanath HR (1981) Lattice defects in semiconducting $Hg_{1-x}Cd_xTe$ alloys. II. Defect structure of indium – doped $Hg_{0.8}Cd_{0.2}Te$. J Electrochem Soc 128(12):2619–2625. https://doi.org/10.1149/1.2127315
38. Vydyanath HR, Donovan JC and Nelson DA (1981) Lattice defects in semiconducting $Hg_{1-x}Cd_xTe$ alloys. III. Defect structure of undoped $Hg_{0.6}Cd_{0.4}Te$. J Electrochem Soc 128(12):2625–2629. https://doi.org/10.1149/1.2127316
39. Chandra D, Schaake HF, Tregilgas JH, Aqariden F, Kinch MA, Syllaios AJ (2000) Vacancies in $Hg_{1-x}Cd_xTe$. J Electron Mater 29(6):729–731. https://doi.org/10.1007/s11664-000-0215-0
40. Mynbaev KD, Ivanov-Omskii VI (2006) Doping of epitaxial and heterostructures based on HgCdTe. Semiconductors 40(1):1–21. https://doi.org/10.1134/S1063782606010015
41. Irvine SJC, Mullin JB (1981) The growth by MOVPE and characterization of CdxHg1−xTe. J Cryst Growth 55(1):107–115. https://doi.org/10.1016/0022-0248(81)90277-3
42. Tunnicliffe J, Irvine SJC, Dosser OD, Mullin JB (1984) A new MOVPE technique for growth of highly uniform CMT. J Cryst Growth 68(1):245–253. https://doi.org/10.1016/0022-0248(84)90423-8

43. Piotrowski A, Klos K (2007) Metal-Organic vapor deposition of Hg1-xCdxTe fully doped heterostructures without postgrowth anneal for uncooled MWIR and LWIR detectors. J Electron Mater 36(8):1052–1058. https://doi.org/10.1007/s11664-007-0171-z
44. Madejczyk P, Piotrowski A, Kłos K, Gawron W, Rogalski A, Rutkowski J, Mroz W (2009) Surface smoothness improvement of HgCdTe layers grown by MOCVD. Bull Pol Acad Sci Tech Sci 57(2):139–146. https://doi.org/10.2478/V10175-010-0114-3
45. Nishino H, Murakami S, Saito T, Nishijima Y, Takigawa H (1995) Dislocation profiles in MCT (100) on GaAs (100) grown by metalorganic chemical vapor deposition. J Electron Mater 24(5):533–537. https://doi.org/10.1007/BF02657959
46. Maxey CD, Fitzmaurice JC, Lau HW, Hipwood LG, Shaw CS, Jones CL, Capper P (2006) Current status of large-area MOVPE growth of MCT device heterostructures for infrared focal plane arrays. J Electron Mater 35(6):1275–1282. https://doi.org/10.1007/s11664-006-0254-2
47. Chilyasov AV, Moiseev AN, Evstigneev VS, Stepanov BS, Drozdov MN (2016) Growth of Arsenic-doped cadmium telluride epilayers by metalorganic chemical vapor deposition. Inorg Mater 52(12):1210–1214. https://doi.org/10.1134/S0020168516120037
48. Hoke WE, Lemonias PJ (1985) Metalorganic growth of CdTe and HgCdTe epitaxial films at a reduced substrate temperature using diisopropyl telluride. Appl Phys Let 46(4):398–400. https://doi.org/10.1063/1.95591
49. Hoke WE, Lemonias PJ (1986) Low-temperature metalorganic growth of CdTe and HgTe films. Appl Phys Let 48(24):1669–1671. https://doi.org/10.1063/1.96850
50. Ghandhi SK, Bhat IB, Ehsani H, Nucciarone D, Miller G (1989) Low temperature growth of HgTe and HgCdTe using methylallyltelluride. Appl Phys Let 55(2):137–139. https://doi.org/10.1063/1.102124
51. Morris BJ (1986) Photochemical organometallic vapor phase epitaxy of mercury cadmium telluride. Appl Phys Let 48(13):867–869. https://doi.org/10.1063/1.96694
52. Irvine SJC, Bajaj J (1993) In situ characterization techniques for monitoring and control of VPE growth of $Hg_{1-x}Cd_xTe$. Semicond Sci Technol 8(6S):860–871. https://doi.org/10.1088/0268-1242/8/6S/007
53. Irvine S, Capper P (eds) (2020) Metalorganic Vapor Phase Epitaxy (MOVPE): growth, materials properties and applications. Wiley, Chichester, p 558
54. Korenstein R, Hallock P, MacLeod B, Hoke W, Oguz S (1990) The influence of crystallographic orientation on gallium incorporation in HgCdTe grown by metalorganic chemical vapor deposition on GaAs. J Vac Sci Technol A 8(2):1039–1044. https://doi.org/10.1116/1.576958
55. Capper PAC, Whiffin BC, Easton CD, Maxey IK (1988) Group V acceptor doping of $Cd_xHg_{1-x}Te$ layers grown by metalorganic vapour phase epitaxy. Mater Let 6(10):365–368. https://doi.org/10.1016/0167-577X(88)90125-5
56. Easton BC, Maxey CD, Whiffin PAC, Roberts JA, Gale IG, Grainger F, Capper P (1991) Impurities and metal organic chemical-vapor deposition growth of mercury cadmium telluride. J Vac Sci Technol B 9(3):1682–1686. https://doi.org/10.1116/1/585399
57. Maxey CD, Whiffin PAC, Easton BC (1991) MOVPE growth and characterization of doped $Cd_xHg_{1-x}Te$ structures. Semicond Sci Technol 6(12C):C26–C30. https://doi.org/10.1088/0268-1242/6/12C/006
58. Madejczyk P, Piotrowski A, Kłos K, Gawron W, Rutkowski J, Rogalski A (2010) Control of acceptor doping in MOCVD HgCdTe epilayers. Opto-Electron Rev 18(3):271–275. https://doi.org/10.2478/s11772-010-1023-x
59. Capper P, Maxey CD, Whiffin PAC, Easton BC (1989) Incorporation and activation of group V elements in MOVPE-grown $Cd_xHg_{1-x}Te$. J Cryst Growth 97(3–4):833–844. https://doi.org/10.1016/0022-0248(89)90585-X
60. Clerjaud B, Gôte D, Svob L, Marfaing Y, Druilhe R (1993) Hydrogen-acceptor pairing in CdTe epitaxial layers grown by OMVPE. Solid State Comm 85(2):167–170. https://doi.org/10.1016/0038-1098(93)90368-W

61. Mitra P, Tyan YL, Case FC, Starr R, Reine MB (1996) Improved arsenic doping in metalorganic chemical vapor deposition of HgCdTe and in situ growth of high performance long wavelength infrared photodiodes. J Electron Mater 25(8):1328–1335. https://doi.org/10.1007/BF02655028
62. Madejczyk P, Piotrowski A, Gawron W, Kłos K, Pawluczyk J, Rutkowski J, Piotrowski J, Rogalski A (2005) Growth and properties of MOCVD HgCdTe epilayers on GaAs substrates. Opto-Electron Rev 13(3):239–251
63. Whiteley JS, Koppel P, Conger VL, Owens KE (1988) Annealing and electrical properties of organometallic vapor phase epitaxy-interdiffused multilayer process grown HgCdTe. J Vac Sci Technol A 6(4):2804–2807. https://doi.org/10.1116/1.575511
64. Sidorov YG, Dvoretski SA, Mikhailov NN, Yakushev MV, Varavin VS, Antsiferov AP (2000) Molecular-beam epitaxy of narrow-band CdHgTe. Equipment and technology. J Opt Technol 67(1):31–37. https://doi.org/10.1364/JOT.67.000031
65. Svitashev KK, Dvoretsky SA, Sidorov YG, Shvets VA, Mardezhov AS, Nis IE et al (1994) The growth of high-quality MCT films by MBE using in situ ellipsometry. Cryst Res Tech 29(7):931–937. https://doi.org/10.1002/crat.2170290703
66. Vilela MF, Buell AA, Newton MD, Venzor GM, Childs AC, Peterson JM et al (2005) Control and growth of middle wave infrared (MWIR) $Hg_{1-x}Cd_xTe$ on Si by molecular beam epitaxy. J Electron Mater 34(6):898–904. https://doi.org/10.1007/s11664-005-0039-z
67. Shvets VA, Mikhailov NN, Dvoretskii SA (2011) Growing of HgCdTe heterostructures with in situ elipsometric control. Optoelectron Instrument Proc 47(5):426–435. https://doi.org/10.3103/S8756699011050220
68. Mikhailov NN (2005) PhD Thesis, Moleculyarno-luchevaya epitaksiya geterostructur CdxHg1-xTe na podlazhrfh GaAs dlya infrakrasnyh fotopriemnikov, Institute of Semiconductor Physics, Novosibirsk. (in Russian)
69. Blinov VV, Goryaev EP, Dvoretsky SA, Mikhailov NN, Myasnikov VN, Sidorov YG, Stenin SI (1998) Usroystvo dlya moleculyarno-luchevoy epitaxii. RU Patent 2111291. May 20 1998 (in Russian)
70. Sivananthan S, Chu X, Reno J, Faurie JP (1986) Relation between crystallographic orientation and the condensation coefficients of Hg, Cd and Te during molecular beam epitaxial growth of $Hg_{1-x}Cd_xTe$ and CdTe. J Appl Phys 60(4):1359–1363. https://doi.org/10.1063/1.337310
71. Almeida LA, Groenert M, Markunas J, Dinan JH (2006) Influence of substrate orientation on the growth of HgCdTe by molecular beam epitaxy. J Electron Mater 35(6):1214–1218. https://doi.org/10.1007/s11664-006-0243-5
72. Koestner RJ, Schaake HF (1988) Kinetics of molecular beam epitaxial HgCdTe growth. J Vac Sci Technol A 6:2834–2839. https://doi.org/10.1116/1.575611
73. Varavin VS, Dvoretsky SA, Liberman VI, Mikhailov NN, Sidorov YG (1996) Molecular beam epitaxy of high quality Hg1−xCdxTe films with control of the composition distribution. J Cryst Growth 159:1161–1166. https://doi.org/10.1016/0022-0248(95)00845-4
74. Rujirawat S, Almeida LA, Chen YP, Sivananthan S, Smith DJ (1997) High quality large-area CdTe(211)B on Si(211) grown by molecular beam epitaxy. Appl Phys Lett 71:1810–1812. https://doi.org/10.1063/1.119406
75. Sidorov YG, Dvoretskii SA, Varavin VS, Mikhailov NN, Yakushev MV, Sabinina IV (2001) Molecular-beam epitaxy of Mercury–Cadmium–Telluride solid solutions on alternative substrates. Semiconductors 35(9):1045–1053. https://doi.org/10.1134/1.14035694
76. Zanatta JP, Ferret P, Theret G, Million A, Wolny M, Chamonal JP, Destefanis G (1998) Heteroepitaxy of HgCdTe (211)B on Ge substrates by molecular beam epitaxy for infrared detectors. J Electron Mater 27:542–545. https://doi.org/10.1007/s11664-998-0012-8
77. Dvoretsky SA, Mikhailov NN, Ikusov DG, Kartashev VA, Kolesnikov AV, Sabinina IV, Sidorov YG, Shvets VA (2020) The growth of CdTe on GaAs substrate by MBE. In: Nanai L, Samantara A, Ratha S (eds) Method for film synthesis and coating procedures. INTECH, p 704. https://doi.org/10.5772/intechopen.73994

78. Wenisch J, Eich D, Lutz H, Schallenberg T, Wollrab R, Ziegler J (2012) MBE growth of MCT on GaAs substrates at AIM. J Electron Mater 41:2828–2832. https://doi.org/10.1007/s11664-012-2113-7
79. Erdem Arkun F, Edwall DD, Ellsworth J, Douglas S, Zandian M, Carmody M (2017) Characterization of HgCdTe films grown on large-area CdZnTe substrates by molecular beam epitaxy. J Electron Mater 46:5374–5378. https://doi.org/10.1007/s11664-017-5441-9
80. Reddy M, Peterson JM, Vang T, Franklin JA, Vilela MF, Olsson K et al (2011) Molecular beam epitaxy growth of HgCdTe on large-area Si and CdZnTe substrates. J Electron Mater 40: 1706–1716. https://doi.org/10.1007/s11664-011-1665-2
81. Ziegler J, Wenisch R, Breiter D, Eich H, Figgemeier P, Fries HL, Wollrab R (2014) Improvements of MCT MBE growth on GaAs improvements of MCT MBE growth on GaAs. J Electron Mater 43:2935–2940. https://doi.org/10.1007/s11664-014-3149-7
82. Varavin VS, Vasilyev VV, Dvoretskii SA, Mikhailov NN, Ovsyuk VN, Sidorov YG et al (2003) HgCdTe epilayers on GaAs: growth and devices. Opto-Electron Rev 11(2):99–111; *Proc. SPIE*, 5136, 381 (2003). https://doi.org/10.1117/12.519761
83. Sidorov YG, Anciferov AP, Varavin VS, Dvoretsky SA, Mikhailov NN, Yakushev MV et al (2016) Molecular beam epitaxy of $Cd_xHg_{1-x}Te$. In: Latyshev AV, Dvurechenskii AV, Aseev AL (eds) Advances in semiconductor nanostructures. Growth, characterization, properties and applications. Elsevier, p 297. https://doi.org/10.1016/B978-0-12-810512-2.00012-3
84. Zanatta JP, Badano G, Ballet P, Largeron C, Baylet J, Gravrand O et al (2006) Molecular beam epitaxy growth of HgCdTe on Ge for third-generation infrared detectors. J Electron Mater 35: 1231–1236. https://doi.org/10.1007/s11664-006-0246-2
85. Vilela MF, Lofgreen DD, Smith EPG, Newton MD, Venzor GM, Peteson JM et al (2008) LWIR HgCDTe detectors grown on Ge substrates. J Electron Mater 37(9):1465–1470. https://doi.org/10.1007/s11664-008-0443-2
86. Reddy M, Peterson JM, Vang T, Franklin JA, Vilela MF, Olsson K et al (2011) Molecular beam epitaxy growth of HgCdTe on large-area Si and CdZnTe substrates. J Electron Mater 40(8):1706–1716. https://doi.org/10.1007/s11664-011-1665-2
87. Reddy M, Jin X, Lofgreen DD, Franklin JA, Peterson JM, Vang T et al (2019) Demonstration of high-quality MBE HgCdTe on 8-inch wafers. J Electron Mater 48(10):6040–6044. https://doi.org/10.1007/s11664-019-07246-y
88. Yakushev MV, Brunev DV, Varavin VS, Vasilyev VV, Dvoretskii SA, Marchishin IV et al (2011) HgCdTe heterostructures on Si (310) substrates for mid infrared focal plane arrays. Semiconductors 45(3):385–391. https://doi.org/10.1134/S1063782611030250
89. Varavin VS, Vasilyev VV, Guzev AA, Dvoretsky SA, Kovchavtsev AP, Marin DV et al (2016) CdHgTe heterostructures for new generation IR photodetectors operating at elevated temperatures. Semiconductors 50(12):1626–1629. https://doi.org/10.1134/S1063782616120265
90. Johnson SM, Buell AA, Vilela MF, Peterson JM, Varesi JB, Newton MD et al (2004) HgCdTe/Si materials for long wavelength infrared detectors. J Electron Mater 33(6): 526–530. https://doi.org/10.1007/s11664-004-0041-x
91. Simingalam S, Brill G, Wijewarnasuriya P, Rao MV (2015) Low temperature, rapid thermal cycle annealing of HgCdTe grown on CdTe/Si. J Electron Mater 44(9):1321–1326. https://doi.org/10.1007/s11664-014-3542-2
92. Wijewarnasuriya PS, Zandian M, Young DB, Waldrop J, Edwall DD, Mclevige WV et al (1999) Microscopic defects on MBE grown LWIR $Hg_{1-x}Cd_xTe$ material and their impact on device performance. J Electron Mater 28(6):649–653. https://doi.org/10.1007/s11664-999-0048-4
93. Sabinina IV, Gutakovsky AK, Sidorov YG, Dvoretsky SA, Kuzmin VD (1992) Defect formation during growth of CdTe (111) and HgCdTe films by molecular beam epitaxy. J Cryst Growth 117:238–243. https://doi.org/10.1016/0022-0248(92)90752-5
94. Aoki T, Chang Y, Badano G, Zhao J, Grein C, Sivananthan S, Smith DJ (2003) Electron microscopy of surface-crater defects on HgCdTe/CdZnTe(211)B epilayers grown by

molecular beam epitaxy. J Electron Mater 32(7):703–709. https://doi.org/10.1007/s11664-003-0056-8
95. Sabinina IV, Gutakovsky AK, Sidorov YG, Latyshev AV (2005) Nature of V-shaped defects in HgCdTe epilayers grown by molecular beam epitaxy. J Cryst Growth 274:339–346. https://doi.org/10.1016/j.jcrysgro.2004.10.053
96. Wijewarnasuriya PS, Lange MD, Sivananthan S, Faurie JP (1994) Carrier recombination in indium doped HgCdTe(211)B epitaxial layers grown by molecular beam epitaxy. J Appl Phys 75:1005–1009. https://doi.org/10.1063/1.356506
97. Bakhtin PA, Dvoretskii SA, Varavin VS, Korobkin AP, Mikhailov NN, Sabinina IV, Sidorov YG (2004) Effect of low-temperature annealing on electrical properties of n-HgCdTe. Semiconductors 38(10):1172–1175. https://doi.org/10.1134/1.1808823
98. Sidorov GY, Mikhailov NN, Varavin VS, Sidorov YG, Dvoretskii SA (2008) Effect of the arsenic cracking zone temperature on the efficiency of arsenic incorporation in CdHgTe films in molecular-beam epitaxy. Semiconductors 42(6):651–654. https://doi.org/10.1134/S1063782608060043
99. Srivastav V, Pal R, Vyas HP (2005) Overview of etching technologies used for HgCdTe. Opto-Electron Rev 13(3):197–211
100. Kotina IM, Tukhkonen LM, Patsekina GV, Shchukarev AV, Gusinskii GM (1998) Study of CdTe etching process in alcoholic solutions of bromine. Semicond Sci Technol 13(8):890–894. https://doi.org/10.1088/0268-1242/13/8/011
101. Causier A, Gerard I, Bouttemy M, Etchberry A, Pautet C, Baylet J, Mollard L (2011) Wet etching of HgCdTe in aqueous bromine solution. J Electron Mater 40(8):1823–1829. https://doi.org/10.1007/s11664-011-1660-7
102. Belas E, Grill R, Franc J, Toth A, Höschl P, Sitter H, Moravec P (1996) Determination of the migration energy of Hg interstitials in (HgCd)Te from ion milling experiments. J Cryst Growth 159(1):1117–1122. https://doi.org/10.1016/0022-0248(95)00696-6
103. Izhnin II, Mynbaev KD, Voitsekhovskii AV, Korotaev AG, Fitsych OI, Pociask-Bialy M (2017) Ion etching of HgCdTe: properties, patterns and use as a method for defect studies. Opto-Electron Rev 25(2):148–170. https://doi.org/10.1016/j.opelre.2017.03.007
104. Liu L, Chen Y, Ye Z, Ding R (2018) A review on plasma-etch-process induced damage of HgCdTe. Infrared Phys Technol 90:175–185. https://doi.org/10.1016/j.infrared.2018.03.009
105. Keller RC, Seelmann-Eggerbert M, Richter HJ (1995) Reaction chemistry and resulting surface structure of HgCdTe etched in CH_4/H_2 and H_2 ECR plasmas. J Electron Mater 24(9):1155–1160. https://doi.org/10.1007/BF02653068
106. Eddy CR, Leonhardt JD, Shamamiam VA, Holm RT, Glembocki OJ, Meyer JR, Hogman CA, Butler JE (1996) Characterization of CH_4/H_2 /Ar high density plasma etch process for HgCdTe. MRS Online Proc Library 450:275. https://doi.org/10.1557/PROC-450-275
107. Boulard E, Cardinaud C, Baylet JJ (2009) Effect of Ar and N_2 addition on CH_4-H_2 based chemistry inductively coupled plasma etching of HgCdTe. J Vac Sci Technol A 27(4):855–861. https://doi.org/10.1116/1.3147219
108. Keller RC, Seelmann-Egelbert M, Richter JH (1995) Addition of N_2 as a polymer deposition inhibitor in CH_4/H_2 electron cyclotron plasma etching of $Hg_{1-x}Cd_xTe$. Appl Phys Let 67:3750–3752. https://doi.org/10.1063/1.115372
109. Smith EGP, Gleason JK, Pham LT, Patten EA, Welkowsky MS (2003) Inductivity coupled plasma etching of HgCdTe. J Electron Mater 32(7):816–820. https://doi.org/10.1007/s11664-003-0076-4
110. Smith EGP et. al., (2007) J Electron Mater 36(8):884
111. Izhnin II, Mynbaev KD, Voitsechovskii AV, Korotaev AG, Fitsych OI, Pociask-Bialy M (2017) Ion etching of HgCdTe: properties, pattern and use as a method for defect studies. Opto-Electron Rev 25(2):148–170. https://doi.org/10.1016/j.opelre.2017.03.007
112. Belas E, Franc J, Toth A, Moravec P, Grill R, Sitter H, Höschl P (1996) Type conversion of p-(HgCd)Te using and Ar reactive ion etching. Semicond Sci Technol 11(7):1116–1120. https://doi.org/10.1088/0268-1242/11/7/024

113. Gorshkov DV, Sidorov GY, Varavin VS, Sabinina IV, Yakushev MV (2020) Reconversion of the CdHgTe conductivity type after plasma etching process at low temperature. Appl Phys Let 116(8):082102. https://doi.org/10.1063/1.5136265
114. Sidorov GY, Gorshkov DV, Sidorov YG, Sabinina IV, Varavin VS (2020) Effect of surface treatment on the charge density at the interface between CdHgTe epitaxial films and Al_2O_3 grown by atomic layer deposition. Optoelectron Instrument Proc 56(5):492–497. https://doi.org/10.3103/S875669902005012X
115. Westerhout R, Musca C, Antoszewski J, Dell JM, Faraone L (2007) Investigation of 1/f noise mechanisms in midwave infrared HgCdTe gated photodiodes. J Elecrtron Mater 36(8): 884–889. https://doi.org/10.1007/s11664-007-0120-x
116. Zakirov ER, Kesler VG, Sidorov GY, Prosvirin IP, Gutakovsky AK, Vdovin VI (2019) XPS investigation of the ALD Al_2O_3/HgCdTe heterointerface. Semicond Sci Technol 34(6): 065007. https://doi.org/10.1088/1361-6641/ab1961
117. Rogalski A, Adamiec K, Rutkowski J (eds) (2000) Narrow-gap semiconductor photodiodes. SPIE Press, Bellingham
118. Kovchavtsev AP, Sidorov GY, Nastovjak AE, Tsarenko AV, Sabinina IV, Vasilyev VV (2017) Mercury cadmium telluride surface passivation by the thin alumina film atomic-layer deposition. J App Phys 121(12):125304. https://doi.org/10.1063/1.4978967
119. Nemirovsky Y, Bahir G (1989) Passivation of mercury cadmium telluride surfaces. J Vac Sci Technol A 7(2):450–459. https://doi.org/10.1116/1.576202
120. Nemirovsky Y, Burstein L (1984) Anodic sulfide films on $Hg_{1-x}Cd_xTe$. AppI Phys Lett 44: 443. https://doi.org/10.1063/1.94760
121. Nemirovsky Y, Burstein L (1985) Interface of p-type $Hg_{1-x}Cd_xTe$ passivated with native sulfides. J Appl Phys 58:366. https://doi.org/10.1063/1.335686
122. Spicer WE, Silberman JA, Lindau I, Chen A-B, Sher A, Wilson JA (1983) Band gap variation and lattice, surface, and interface "instabilities" in $Hg_{1-x}Cd_xTe$ and related compounds. J Vac Sci Technol A 1(3):1735–1743. https://doi.org/10.1116/1.572206
123. Wilson JA, Cotton VA (1985) Electrical properties of the SiO_2:HgCdTe interface. J Vac Sci Technol A 3(1):199–202. https://doi.org/10.1116/1.573200
124. Castagne R, Vapaille A (1970) Effet des fluctuations spatiales du potential a l'interface SiO2/Si sur les courbes capacite-tension d'une structure MOS. C R Acad Sci (Paris) 270:1347
125. Bhan RK, Srivastava V, Saxena RS, Sareen L, Pal R, Sharma RK (2010) Improved high resistivity ZnS films on HgCdTe for passivation of infrared devices. Infrared Phys Technol 53 (I.5):404–409. https://doi.org/10.1016/j.infrared.2010.07.008
126. Biryulin PV, Dudko SA, Konovalov SA, Pelevin YA, Turinov VI (2003) Investigation of the ZnS-CdHgTe interface. Semiconductors 37(12):1383–1386. https://doi.org/10.1134/1.1634658
127. Whelan MV (1965) Graphical relation between surface parameters of silicon, to be used in connection with MOS-capacitance measurement. Philips Res Rep 20:620–632
128. Zhang J, Umana-Membreno GA, Gu R, Lei W, Antoszewski J, Dell JM, Faraone L (2015) Investigation of ICPECVD silicon nitride films for HgCdTe surface passivation. J Electron Mater 44(9):2990–3001. https://doi.org/10.1007/s11664-015-3703-y
129. Castagné R, Vapaille A (1971) Description of the SiO2-Si interface properties by means of very low frequency MOS capacitance measurements. Surf Sci 28(1):157–193. https://doi.org/10.1016/0039-6028(71)90092-6
130. Gorshkov DV, Sidorov GY, Sabinina IV, Sidorov Y, Marin DV, Yakushev MV (2020) The effect of the growth temperature on the passivating properties of the Al_2O_3 films formed by atomic layer deposition on the CdHgTe surface. Technical Phys Let 46(8):741–744. https://doi.org/10.1134/S1063785020080064
131. Voitsekhovskii AV, Nesmelov SN, Dzyadukh SM (2017) Admittance measurements in the temperature range (8−77) K for characterization of MIS structures based on MBE n-$Hg_{0.78}Cd_{0.22}Te$ with and without graded-gap layers. J Phys Chem Sol 102:42–48. https://doi.org/10.1016/j.jpcs.2016.10.015

132. Fu R, Pattison J, Chen A, Nayfeh O (2012) Mercury cadmium telluride (HgCdTe) passivation by advanced thin conformal Al_2O_3 films. Proc SPIE 8353:885–891. https://doi.org/10.1117/12.918605
133. Banerjee S, Su P, Dahal R, Bhat IB, Bergeson JD, Blissett C, Aqariden F, Hanyaloglu B (2014) Surface passivation of HgCdTe using low-pressure chemical vapor deposition of CdTe. J Electron Mater 43:3012–3017. https://doi.org/10.1007/s11664-014-3178-2
134. Nemirovsky Y, Mainzer N, Weiss E (1994) Passivation of HgCdTe. In: Capper P (ed) Properties of narrow gap cadmium based compounds. INSPEC, IEE, London, p 284
135. Kumar V, Pal R, Chaudhury PK, Sharma BL, Gopal V (2005) A CdTe passivation process for long wavelength infrared HgCdTe photodetectors. J Electron Mater 34(9):1225–1229. https://doi.org/10.1007/s11664-005-0267-2
136. Tennant WE, Cockrum CA, Gilpin JB, Kinch MA, Reine MB, Ruth RP (1992) Key issues in HgCdTe based focal plane arrays: an industry perspective. J Vac Sci Technol B 10:1359. https://doi.org/10.1116/1.585869
137. Rogalski A (2020) HgCdTe photodetectors. In: Tournir E, Gerutti L (eds) Mid-infrared optoelectronics. Materials, devices and applications. Elsevier Duxford, p 235
138. Nemirovsky Y, Amir N (1997) Surfaces/interfaces of narrow-gap II-VI compounds. In: Capper P (ed) *Narrow-Gap II-VI compounds for optoelectronic and electromagnetic applications*. Chapman & Hall, London, p 291
139. Spicer WE, Friedman DJ, Carey GP (1988) The electrical properties of metallic contacts on $Hg_{1-x}Cd_xTe$. J Vac Sci Technol A 6(4):2746–2751. https://doi.org/10.1116/1.575499
140. Flores F, Tejidor C (1987) On the formation of semiconductor interface. J Phys C Solid State Phys 20(2):145–176. https://doi.org/10.1088/0022-3719/20/2/001
141. Spicer WE, Chye PW, Skeath PR, Su CY, Lindau I (1979) New and unified model for Shottky barrier and III-V insulator interface state formation. J Vac Sci Technol 16(5):1422–1433. https://doi.org/10.1116/1.57015
142. Spicer WE, Lindau I, Skeath PR, Chye PW, Su CY (1980) Unified defect model and beyond. J Vac Sci Technol 17(5):1019–1027. https://doi.org/10.1116/1.570583
143. Heine V (1965) Theory of surface states. Phys Rev 138(6A0):A1689–A1698. https://doi.org/10.1103/Phys.Rev.138.A1689
144. Freeouf JL, Woodall JM (1981) Schottky barrier: an effective work function model. Appl Phys Lett 39:727. https://doi.org/10.1063/1.92863
145. Long D, Schmit JL (1970) In: Willardson RK, Beer AC (eds) Semiconductors and semimetals, vol 5. Academic, New York, p 175
146. Rogalski A, Piotrowski J (1988) Intrinsic infrared detectors. Prog Quant Electron 12:87–289. https://doi.org/10.1016/0079-6727(88)90001-8
147. Reine MB (2001) Photovoltaic detectors in MCT. In: Capper P, Elliott CT (eds) Infrared detectors and emitters: materials and devices. Kluwer Academic Publishers, Boston, p 313
148. Leech PW, Reeves GK (1992) Specific contact resistance of indium ohmic contacts to n-type $Hg_{1-x}Cd_xTe$. J Vac Sci Technol A 10(1):105–109. https://doi.org/10.1116/1.578121
149. Beck WA, Davis GD, Goldberg AC (1990) Resistance and 1/f noise of Au, Al, and Ge contacts to (Hg,Cd)Te. J Appl Phys 67:6340–6346. https://doi.org/10.1063/1.345154
150. Storm W, Altebockwinkel M, Wiedmann L, Benninghoven A, Ziegler J, Bauer A (1991) Depth profile analysis of Pt, Cu, and Au overlayers on p-$Hg_{1-x}Cd_xTe$. J Vac Sci Technol A 9(1):14–20. https://doi.org/10.1116/1.577115
151. Sizov F, Tsybrii Z, Apats'ka M, Dmytruk N, Slipokurov V, Bunchuk S et al (2020) Ohmic metal/ $Hg_{1-x}Cd_xTe$ ($x \approx 0.3$) contacts. Semicond Sci Technol 35:125030. https://doi.org/10.1088/1361-6641/abc0f7
152. Piotrowski A, Madejczyk P, Gawron W, Kłos K, Romanis M, Grudzień M, Rogalski A, Piotrowski J (2004) MOCVD growth of $Hg_{1-x}Cd_xTe$ heterostructures for uncooled infrared photodetectors. Opto-Electron Rev 12(4):453–458

153. Janik E, Triboulet R (1983) Ohmic contacts to p-type cadmium telluride and cadmium mercury telluride. J Phys D Appl Phys 16(12):2333–2340. https://doi.org/10.1088/0022-3727/16/12/011
154. Bubulac LO, Lo DS, Tennant WE, Edwall DD, Chen JC, Ratusnik J, Robinson JC, Bostrup G (1987) Ion implanted junction formation in $Hg_{1-x}Cd_xTe$. J Vac Sci Technol A 5(5): 3166–3170. https://doi.org/10.1116/1.574861
155. Baker IM (2017) II-VI narrow bandgap semiconductors: optoelectronic. In: Kasap S, Capper P (eds) Handbook of electronic and photonic materials II-VI narrow bandgap semiconductors: optoelectronics, 2nd edn. Springer, Leipzig, p 867
156. Lei W, Antoszewski J, Faraone L (2015) Progress, challenges, and opportunities for HgCdTe infrared materials and detectors. Appl Phys Rev 2:041303. https://doi.org/10.1063/1.4936577
157. Dutton DT, O'Keefe E, Capper P, Jones CL, Mugford S, Ard C (1993) Type conversion of $Cd_xHg_{1-x}Te$ grown by liquid phase epitaxy. Semicond Sci Technol 8:S266–S269. https://doi.org/10.1088/0268-1242/8/1S/058
158. Jenner MD, Blackman MV (1982) Method of manufacturing an infrared detector device. US Patent. 4,318,217, 9 March 1982
159. Blackman MV, Charlton DE, Jenner MD, Purdy DR, Wotherspoon JTM, Elliot CT, White AM (1987) Type conversion in $Hg_{1-x}Cd_xTe$ by ion beam treatment. Electron Lett 23(19:978–979. https://doi.org/10.1049/el:19870688
160. Mynbaev KD, Ivanov-Omski VI (2003) Modification of $Hg_{1-x}Cd_xTe$ properties by low energy ions. Semiconductors 37(10):1127–1150. https://doi.org/10.1134/1.1619507
161. Baker IM, Ballinga RA (1984) Photovoltaic CdHgTe-silicon hybrid focal planes. Proc SPIE 510:121–129. https://doi.org/10.1117/12.945014
162. Agnihorti OP, Lee HC, Yang K (2002) Plasma induced type conversion in mercury cadmium telluride. Semicond Sci Technol 17:R11–R19
163. Destefanis G (1988) Electrical doping of HgCdTe by ion implantation and heat treatment. J Cryst Growth 86(1–4):700–722. https://doi.org/10.1016/0022-0248(90)90798-P
164. Marchishin IV, Sabinina IV, Sidorov GY, Yakushev MV, Varavin VS, Remesnik VG et al (2020) HgCdTe-based 640 × 512 matrix midwave infrared photodetector. J Commun Technol Electron 65(3):316–320. https://doi.org/10.1134/S1064226920030122
165. Zverev AV, Suslyakov AO, Sabinina IV, Sidorov GY, Yakushev MV, Kuzmin VD et al (2019) Photodetectors with 384 × 288 matrix elements for the infrared range of 8–10 microns. J Commun Technol Electron 64(9):1024–1029. https://doi.org/10.1134/S1064226919090171
166. Vuillermet M, Billon-Lanfrey D, Reibel Y, Manissadjian A, Mollard L, Baier N, Gravrand O, Destéfanis G (2012) Status of MCT focal plane arrays in France. Proc. of SPIE 8353:83532K
167. Figgemeier H, Hanna S, Eich D, Fries P, Mahlein K-M, Wenisch J et al (2017) State-of-the-Art MCT photodiodes for cutting-edge sensor applications by AIM. Proc of SPIE 10177: 101771K. https://doi.org/10.1117/12.2261925
168. Foyt AG, Harman TC, Donnelly JP (1971) Type conversion and n–p junction formation in CdxHg1−xTe produced by proton bombardment. Appl Phys Lett 18(8):321–323. https://doi.org/10.1063/1.1653679
169. Kozlowski LJ, Bailey RB, Cabelli SC, Cooper DE, McComas G, Vural K, Tennant WE (1992) 640×480 PACE HgCdTe FPA. Proc SPIE 1735:163–173. https://doi.org/10.1117/12.138620
170. Lutz H, Breiter R, Rutzinger S, Schallenberg T, Wendler J, Ziegler J (2013) High-performance IR detector modules for army applications. Proc SPIE 8704:87040A. https://doi.org/10.1117/12.2015714/
171. Bubulac LO (1988) Defects, diffusion and activation in ion implanted HgCdTe. J Cryst Growth 86(1–4):723–734. https://doi.org/10.1016/0022-0248(90)90799-Q
172. Bubulac LO, Tennant WE (1987) Role of Hg in junction formation in ion-implanted HgCdTe. Appl Phys Lett 51(5):355–357. https://doi.org/10.1063/1.98439
173. Bubulac LO, Lo DS, Tennant WE, Edwall DD, Chen JC, Ratusnik J, Robinson JC, Bostrup G (1987) P on n ion-implanted junctions in liquid phase epitaxy HgCdTe layers on CdTe substrates. Appl Phys Lett 50:1586–1589. https://doi.org/10.1063/1.97788

174. Mollard L, Destefanis G, Baier N, Rothman J, Ballet P, Zanatta JP, Tchagaspanian M, Papon AM, Bourgeois G, Barnes JP (2009) Planar p-on-n HgCdTe FPAs by Arsenic Ion Implantation. J Electron Mater 38(9):1805–1813. https://doi.org/10.1007/s11664-009-0829-9
175. Eich D, Schirmacher W, Hanna S, Mahlein KM, Fries P, Figgemeier H (2017) Progress of MCT detector technology at AIM towards smaller pitch and lower dark current. J Electron Mater 46(9):5448–5457. https://doi.org/10.1007/s11664-017-5596-4
176. Kovchavtsev AP, Guzev AA, Tsarenko AV, Panova ZV, Yakushev MV, Marin DV et al (2015) The reverse current temperature dependences of SWIR CdHgTe "p-on-n" and "n-on-p" junctions. Infrared Phys Technol 73:312–315
177. Varavin VS, Sabinina IV, Sidorov GY, Marin DV, Remesnik VG, Predein AV et al (2020) Photodiodes based on p-on-n junctions formed in MBE-grown n-type MCT absorber layers for the spectral region 8 to 11 μm. Infrared Phys Technol 105:103182. https://doi.org/10.1016/j.infrared.2019.103182
178. Rogalski A (2005) HgCdTe infrared detector material: history, status and outlook. Rep Prog Phys 68:2267–2336
179. Destefanis G, Baylet J, Ballet P, Castelein P, Rothan F, Gravrand O, Rothman J, Chamonal JP, Million A (2007) Status of HgCdTe bicolor and dual-band infrared focal plane arrays at LETI. J Electron Mater 36(8):1031–1044. https://doi.org/10.1007/s11664-007-0168-7
180. Kinch MA (2000) Fundamental physics of infrared detector materials. J Electron Mater 29(6):809–817. https://doi.org/10.1007/s11664-000-0229-7
181. Krishnamurthy S, Casselman TN (2000) A detailed calculation of the auger lifetime in p-type HgCdTe. J Electron Mater 29(6):828–831. https://doi.org/10.1007/s11664-000-0232-z
182. Wollrab R, Bauer A, Bitterlich H, Bruder M, Hanna S, Lutz H, Mahlein K-M, Schallenberg T, Ziegler J (2011) Planar n-on-p HgCdTe FPAs for LWIR and VLWIR applications. J Electron Mater 40(8):1618–1623. https://doi.org/10.1007/s11664-011-1659-0
183. Haiml M, Eich D, Fick W, Figgemeier H, Hanna S, Mahlein M, Schirmacher W, Thöt R (2016) Low dark current LWIR HgCdTe focal plane arrays at AIM. Proc SPIE 9881:988116. https://doi.org/10.1117/12.2229027
184. Hanna S, Eich D, Mahlein M, Fick W, Schirmacher W, Thöt R et al (2016) MCT-based LWIR and VLWIR 2D focal plane arrays for low dark currents application at AIM. J Electron Mater 45(9):4542–4551. https://doi.org/10.1007/s11664-016-4523-4